Reprinted from the *Encyclopedia of Fluid Mechanics*. Copyright © 1986 by Gulf Publishing Company, P.O. Box 2608, Houston, Texas 77001. All rights reserved.

CHAPTER 8

BUBBLE GROWTH IN SUPERHEATED LIQUID DROPLETS

C. T. Avedisian

Sibley School of Mechanical and Aerospace Engineering
Cornell University
Ithaca, New York, USA

CONTENTS

INTRODUCTION

If two immiscible liquids of different volatility are mixed such that one of the liquids (the volatile one, hereafter referred to as liquid 1) is dispersed in the other (liquid 2) in the form of droplets, the droplets may be heated by direct contact heat transfer across the liquid/liquid interface. This heat may be transferred by

1. Conduction or convection
2. Nucleate boiling
3. Film boiling

In the absence of preferred nucleation sites, single-phase conduction or convection could exist far beyond the normal saturation state of liquid 1. In this event liquid 1 is said to become superheated. The stable, superheated state can exist as long as the droplet does not come in contact with a vapor phase with which it is in equilibrium. An upper limit to the temperature any liquid can sustain at a given pressure (or a lower limit of pressure at a given temperature) exists at which

a phase change must occur. This temperature is called the *superheat limit*. At this temperature an intrinsic phase transition is initiated by the molecular processes of homogeneous nucleation within the bulk of the encapsulated droplet. These processes are characterized by creation of a vapor phase within bulk liquid in the form of tiny (~ 10 Å diameter) bubbles (critical size nuclei) such that they are in metastable equilibrium with the surrounding liquid. Subsequent growth of these initial bubbles completes the phase transition process and is manifested by the boiling-up of the superheated liquid droplet. Two steps in the phase change process relevant to superheated liquid droplets are therefore

1. An initial stage during which microscopic bubbles form within the droplet by molecular processes.
2. A second or bubble growth stage during which the initial microscopic bubbles grow as the liquid droplet vaporizes.

Detailed discussions of both stages are given in this chapter.

Bubble growth beyond the critical size is governed by, in turn, the effects of molecular evaporation across the phase boundary, surface tension, liquid inertia, and thermal diffusion. The compendium of these processes is manifested by the macroscopic behavior of the droplets when they vaporize. Superheated droplets may vaporize in an explosive-like manner and generate blast waves in the surrounding liquid, or boil quiescently as characterized by a comparatively gradual disappearance of the liquid phase and a concomitant emergence of a vapor bubble within the droplet. What little is known about the intensity of vaporization of droplets at their superheat limit suggests that boiling intensity is influenced by such factors as ambient pressure in the field liquid, and physical properties.

This chapter reviews the processes of initial bubble formation and growth within liquid droplets at the superheat limit. The essential configuration considered is that of droplets of a pure volatile liquid (liquid 1) encapsulated in an ambient nonvolatile field liquid (liquid 2) of infinite extent. A summary of applications in which this configuration may be encountered in industrial settings is given in the next section. The problem is then formulated in more formal terms in the following section. A review of the mechanism by which bubbles are created within superheated liquids is presented in the next section, and the bubble growth problem is then discussed. Those aspects of bubble growth in infinite media related to the present problem are reviewed and modifications to the classical theories required by the finite mass of the vaporizing liquid are discussed. Finally, experimental methods used to provide the foundation of our understanding of bubble nucleation and growth within superheated liquid droplets are described in the final section.

APPLICATIONS

The energy released by a liquid at its limit of superheat is approximately equivalent to the sensible heat above normal saturation. If a significant fraction of this energy appears in the form of a thermal detonation wave, or if bubbles grow at a rate which exceeds the ability of the surrounding liquid to acoustically respond, the resulting phase transition is called a "vapor explosion." This energy is orders of magnitude less than that typical of chemical explosions. However, the destructive capability of vapor explosions, produced when a hot nonvolatile liquid comes into intimate contact with a cold volatile liquid, is well documented in the literature [1–3].

To bring a liquid to a state at which there is a high probability for the type of phase transition characteristic of a vapor explosion, the liquid must be devoid of any extraneous nucleation aids. This requirement will most readily (though not always) be satisfied when one liquid is dispersed in another relatively nonvolatile liquid with which it is immiscible. In this case, the "container" for the volatile liquid is the liquid/liquid interface. As the structure of such an interface is not fundamentally different from that of the bulk, the only way for a phase change to occur would be by the same molecular processes as that under which critical size nuclei form. The attendant liquid state will correspond to the deepest possible penetration of the liquid into the domain of metastable states (due account being taken of the effect of the interface)—the limit of superheat—and therefore

create the possibility for a vapor explosion. The precise mechanism of vapor-explosive boiling is not well understood due to a lack of fundamental experiments. Our observations and understanding of the phenomenon are at present rather qualitative. Vapor explosive boiling has been observed during spillage of liquified natural gases on water, preparation and burning of certain alternative fuels, melt-down of nuclear reactor fuel rods in a (as yet hypothetical) nuclear reactor accident, mixing of water and molten metal during the cold mold arc-melting and casting processes, and dissolving of molten salt in water during paper pulping operations. The effect of these explosions have ranged from detrimental, creating a hazard to life and property [3] to potentially beneficial in the case of burning alternative fuels [4, 5].

Conditions which must be satisfied for vapor explosions to occur vary widely and defy generalizations. Though several reviews have recently appeared on the subject [1, 3, 6, 7] no unique mechanism has yet been formulated which can explain all observed phenomena. At present, two necessary conditions for a vapor explosion appear to have received general agreement:

1. A volatile and nonvolatile liquid must come into intimate contact.
2. The temperature of the nonvolatile liquid must be heated to some well defined minimum value which is greater than the boiling point of the volatile liquid—below the threshold temperature, or well above it, vapor explosions will not occur.

The potential for vapor explosions appears to be influenced as much by the way the two liquids are brought together as it is by the heating requirements of the volatile liquid: even if the requisite temperatures are achieved, the method of mixing apparently influences the ability of the volatile liquid to vapor explode.

Other factors such as ambient pressure [8–11], liquid phase composition [12–15], and wetting characteristics of the two liquids [16, 17] have been observed to effect the intensity of boiling after the triggering mechanism of homogeneous nucleation has occurred. Thus by itself, more information must supplement the preceding necessary conditions in order to provide a complete account of the potential for vapor explosions in any interaction between two liquids of different volatilities. The missing information is provided by the dynamics of growth of the initial bubble. These dynamics are influenced by precisely those factors which have been observed to influence the intensity of boiling of a liquid at its superheat limit. Thus we may conjecture a third condition for a vapor explosion which involves bubble growth:

3. Growth of the initial bubble must be sufficiently rapid so as to produce shock waves in the surrounding liquid.

The production of shock or blast waves will usually require a high pressure source (vapor in the bubble itself) and rapid expansion of the liquid/vapor interface. Experimental evidence is suggestive of the necessity of a large enough pressure initially existing in the bubble to support such a shock wave [11, 18].

The necessity to consider the dynamics of bubble growth in connection with vapor explosion has been recognized [e.g. 2, 3, 6, 8, 19]. Little work has, however, been done to quantify the dynamics and heat transfer of bubble growth for the configuration most typical of that encountered as a result of the type of mixing processes already outlined—droplets of one liquid in another. Most previous work in connection with the vapor explosion problem has simplified the problem by not considering the finite extent of the vaporizing liquid-droplet, and has, instead, drawn on results for bubble growth in infinite media to explain qualitative expectations for phenomenon associated with droplets [e.g. 2, 3, 20]. This extension can be valid for certain ranges of the important parameter which will be shown to govern bubble growth in the fifth section. In the general case, however, discrepancies in the growth rate and therefore in the expectations one is likely to predict pertaining to the rate at which the liquid phase vaporizes may be expected.

Finally, the emphasis in this section has been on problems associated with the vapor explosion phenomenon. The present work is, however, not about vapor explosions, but about bubble growth in droplets. The perspective of vapor explosions is convenient to show the importance of the

essential configuration considered in this chapter—droplets of a volatile liquid encapsulated in a nonvolatile liquid of infinite extent. In other respects, the subsequent discussions are not restricted to any unique application.

DESCRIPTION OF THE PROBLEM

Figure 1 illustrates the basic geometry of interest in this chapter. A spherical droplet of a volatile liquid (liquid 1) is suspended in a nonvaporizing nonvolatile liquid of infinite extent (liquid 2). The two liquids are mutually immiscible. The nonvolatility of liquid 2 is such that the potential exists for altering its thermodynamic state to induce intrinsic bubble formation within the bulk of the liquid 1 droplet without jeopardizing the stability of its stable state. This requirement means that the normal saturation temperature of liquid 2 is higher, at a given ambient pressure, than the limit of superheat of liquid 1 at the same pressure. Both liquids are assumed to be free of any extraneous nucleation aids which would tend to initiate a phase transition at conditions less extreme than would be realized in the presence of such aids. Thus we assume an absence of any dissolved gases, unwetted solid particles, or minute gas bubbles in both liquids. In this event the present work will be distinguished from previous studies of phase change in droplets suspended in immiscible liquids [e.g. 21–26] in that the droplets considered here remain liquid at reduced temperatures typically greater than 0.9 corresponding to reduced pressures greater than about 0.04 before boiling.

The problem considered is as follows. At time $t = 0$ a vapor bubble (created by the process of homogeneous nucleation) appears within the bulk of the liquid 1 droplet. The initial temperatures of liquids 1 and 2 are the same and there is no relative motion between the droplet and the field liquid. The unstable equilibrium of the bubble is then perturbed in such a manner that the bubble starts to grow. This perturbation may be an incremental increase in bubble size beyond the initial value corresponding to static equilibrium, and be brought about by a slight reduction of ambient pressure, P_o, or increase in ambient temperature, T_o. Subsequent growth of the bubble consumes the volatile liquid 1 until the initial mass of the droplet is entirely vaporized, after which a vapor

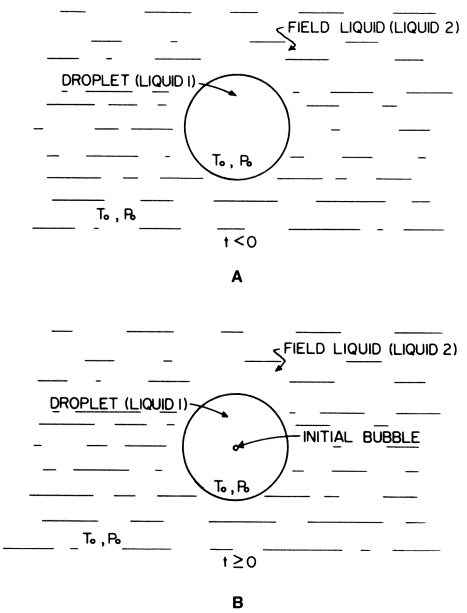

Figure 1. Schematic of droplet/field liquid system illustrating appearance of initial bubble ($t \geq 0$).

bubble of finite size in static equilibrium with liquid 2 remains. The radius of this final bubble is

$$R_f = (1 - \varepsilon)^{-1/3} S_o \tag{1}$$

At this radius, liquid 1 has completely vaporized. For a bubble growing in an infinite medium of liquid 1 (i.e., $S_o \to \infty$), the vapor bubble in principle grows to infinite size.

We now proceed to a discussion of the two main developments pertinent to the present work:

1. The initial conditions for bubble growth characterized by formation of critical size nuclei within the bulk of the droplet.
2. Growth of the initial bubble within the droplet.

A review of those aspects of nucleation theory relevant to predicting the initial conditions for bubble growth is given in the fourth section. A discussion of the bubble growth problem itself is presented in the fifth section.

INITIAL CONDITIONS FOR BUBBLE GROWTH

Superheated Liquids

The terms "superheated liquids" and "limit of superheat" have been used in connection with the initial liquid droplet state at which vaporization is initiated. In this section we wish to more precisely define these terms and to present useful methods for quantitative prediction.

The essential requirement of a superheated liquid is transgression of its normal or saturation phase boundary. "Normal" in this sense is rather arbitrarily defined. By convention the term refers to a special case of equilibrium across a flat-phase boundary, $r \to \infty$ where r is the radius of curvature of the phase boundary.

Figure 2 illustrates two of a possible infinity of paths a pure liquid may follow to transgress its normal-phase boundary. The illustration is made on conventional pressure-temperature and pressure-volume projections on a phase diagram. The two paths illustrated are isobaric heating (a-c) and isothermal decompression (b-c). The latter path is more commonly associated with cavitation processes. The solid line illustrated in Figure 2A which separates the stable liquid and stable vapor regions corresponds to the normal equilibrium boundary. Transgression of this phase boundary implies an absence of a planar interface between the two phases. Hence any vapor present within the superheated liquid regions shown in Figure 2 must be in the form of bubbles ($r < \infty$). The radii of curvature of these bubbles defines the depth of penetration of the liquid in the metastable region.

The initial bubbles are in mechanical equilibrium. Hence,

$$P + \vec{n} \cdot \vec{P}_o = \frac{2\sigma_1}{r} > 0 \tag{2}$$

where $\vec{n}$ is the outward normal to the bubble surface.

The gas pressure, P, is not precisely the same as the equilibrium vapor pressure, $P_s(r \to \infty)$ at temperature T. This is seen by considering the consequences of phase equilibrium across flat and curved phase boundaries illustrated in Figure 3. In both configurations, equality of chemical potentials defines equilibrium. For the planar inteface in Figure 3A

$$\mu'(P_s, T) = \mu''(P_s, T) \tag{3a}$$

while for equilibrium between the gas in the bubble and the surrounding liquid (Figure 3B) at the same temperature,

$$\mu'(P_o, T) = \mu''(P, T) \tag{3b}$$

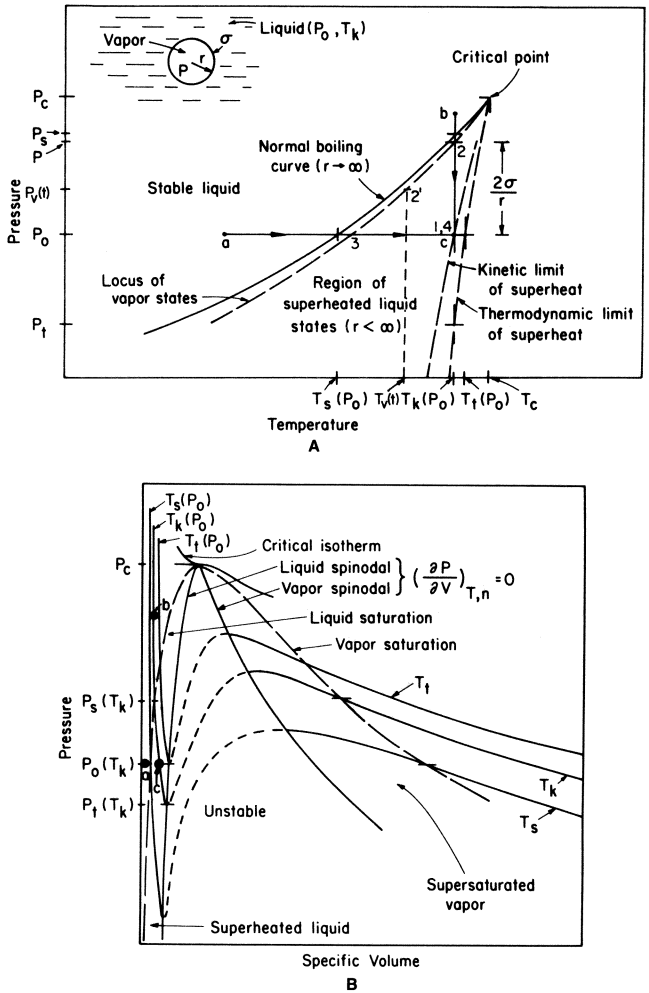

Figure 2. Phase diagram of a pure substance on pressure/temperature (A) and pressure volume (B) projections illustrating the domain of stable, superheated liquid, and unstable states.

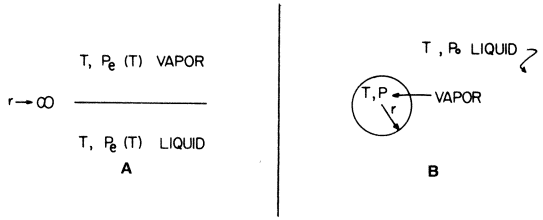

Figure 3. (A) Equilibrium across a flat phase boundary at temperature T; (B) equilibrium across a curved phase boundary (bubble) of radius r and temperature T.

Assuming, for simplicity, the liquid to be incompressible and the gas phase to be ideal, it can be shown that

$$\mu'(P_s, T) - \mu'(P_o, T) = v'(P_s - P_o) \tag{4}$$

and

$$\mu''(P_s, T) - \mu''(P, T) = \mathscr{R}T \ln \frac{P_s}{P} \tag{5}$$

Combining Equations 2–5 yields the desired result:

$$P \simeq P_s \exp\left[\frac{v'}{\mathscr{R}T}(P_o - P_s)\right] \tag{6a}$$

For multicomponent mixtures a similar expression applies where P is the partial pressure of component i in the ideal gas mixture within the bubble [29]

$$P_i \simeq P_s y_{is} \exp\left[\frac{v_i'}{\mathscr{R}T}(P_o - P_s)\right] \tag{6b}$$

P_s is the mixture bubble point pressure of gas-phase composition y_{is}, and v_i' is the corresponding liquid partial molar volume of component i. The exponential terms in Equations 6 are usually very close to one for liquids at the superheat limit. Figure 2 schematically illustrates the locus of vapor states defined by Equation 6a for a pure liquid.

The external liquid pressure, P_o, may be either compressive on the bubble wall or extensive (as in the case of tensile strength measurements [30–32]). In the present discussion we shall be concerned primarily with compressive ambient liquid pressures so that

$$P - P_o = \frac{2\sigma_1}{r} \tag{7}$$

defines the initial equilibrium state of the bubble.

For a vapor bubble $P > P_o$ and $r < \infty$. As a consequence $T(P_o) > T_s(P_o)$. In principle all allowable liquid states are those for which $T(P_o) < T_c$.

Thermodynamic Limit of Superheat

There is an absolute limit to the extent to which a liquid droplet can be isobarically heated. At this limit the liquid is inherently unstable with respect to any small perturbation in its thermodynamic state. The system comprising the liquid then breaks up into two or more portions, the separation being called a phase transition [33].

The limit of stability, or so-called *thermodynamic limit of superheat*, is defined by the basic extreme principle of thermodynamics which asserts that the entropy of an isolated system is a maximum in a stable equilibrium state with respect to small variations of its natural variables, U, V, n_1, n_2 . . . [34]. Alternatively, the Helmholtz function, F, assumes a minimum value in a stable equilibrium state for an open system with respect to variations of T, V, n_1, n_2 . . . . For variations from a stable state (i.e., virtual processes),

$$\Delta F > 0 \tag{8}$$

To explore the consequences of Equation 8, ΔF is expanded in a series about a stable equilibrium state. Such an expansion will accurately represent ΔF if enough terms are retained. Thus, for varia-

tions from a stable state

$$\Delta F = \delta F + \frac{1}{2!}\delta^2 F + \frac{1}{3!}\delta^3 F + \cdots \geq 0 \tag{9}$$

For simplicity we consider the stability of states along an isotherm ($\delta T = 0$). Only small variations in the natural variables are considered such that the first nonvanishing term in Equation 9 is also the largest. The vanishing of certain of these terms defines several thermodynamic states of interest. For systems in a stable state

$$\delta F = 0 \tag{10a}$$

and

$$\delta^2 F \geq 0 \tag{10b}$$

defines stability of this equilibrium. At the thermodynamic limit of superheat equality of Equation 10b applies,

$$\delta^2 F = 0 \tag{11a}$$

and

$$\delta^3 F \geq 0 \tag{11b}$$

defines the stability of states at this limit. A critical point is defined such that

$$\delta^3 F = 0 \tag{12a}$$

and its stability is determined by

$$\delta^4 F \geq 0 \tag{12b}$$

Interest here is in exploring the consequences of Equations 10 and 11 for a liquid not at its critical point (Equation 12). States defined by Equation 11a correspond to the deepest possible penetration of a liquid in the domain of metastable states.

For $F(T, V, n_1, n_2, \ldots)$ Equation 10b can be written ($\delta T = 0$)

$$\begin{aligned}\delta^2 F = {} & F_{vv}(\delta V)^2 + F_{n_1 n_1}(\delta n_1)^2 + F_{n_2 n_2}(\delta n_2)^2 + \cdots + 2[F_{vn_1}\delta V \delta n_1 + F_{vn_2}\delta V \delta n_2 + \cdots \\ & + F_{n_1 n_2}\delta n_1 \delta n_2 + F_{n_1 n_3}\delta n_1 \delta n_3 + \cdots \\ & \vdots \\ & > 0\end{aligned} \tag{13}$$

Subscripts denote differentiation with respect to the indicated variable:

$$F_v = \left.\frac{\partial F}{\partial V}\right|_{T,n_j} = -P \tag{14a}$$

$$F_{n_i} = \left.\frac{\partial F}{\partial n_j}\right|_{T,V,n_j} = \mu_i \tag{14b}$$

$$F_{vn_i} = \left.\frac{\partial^2 F}{\partial V\, \partial n_i}\right|_{T,P,n_j} \tag{14c}$$

Equation 13 is a homogeneous quadratic form. The requirement that it be positive (hence that the state be stable) is equivalent to the requirement that discriminants of the matrix

$$\bar{\bar{A}} \equiv \begin{bmatrix} F_{vv} & F_{vn_1} & F_{vn_2} & \cdots & F_{vn_n} \\ F_{vn_1} & F_{n_1n_1} & F_{n_1n_2} & \cdots & F_{n_1n_n} \\ F_{vn_2} & F_{n_1n_2} & F_{n_2n_2} & \cdots & F_{n_2n_n} \\ \vdots & \vdots & \vdots & & \vdots \\ F_{vn_n} & F_{n_1n_n} & F_{n_2n_n} & & F_{n_nn_n} \end{bmatrix} \tag{15}$$

all be positive [35]. Hence,

$$\begin{aligned} F_{vv} &> 0 \\ \begin{vmatrix} F_{vv} & F_{vn_1} \\ F_{vn_1} & F_{n_1n_1} \end{vmatrix} &> 0 \\ &\vdots \\ |\bar{\bar{A}}| &> 0 \end{aligned} \tag{16}$$

From the Gibbs-Duhem equation we can write that

$$\bar{\bar{A}} \cdot \begin{bmatrix} V \\ n_1 \\ n_2 \\ \vdots \end{bmatrix} = 0 \tag{17}$$

Thus,

$$|\bar{\bar{A}}| = 0 \tag{18}$$

whether or not the state under consideration is stable. The limit of stability is then defined by the discriminant which first vanishes from those constructed from the first $n - 1$ rows and columns of the $n \times n$ matrix $\bar{\bar{A}}$. It can be shown that this discriminant will always be the determinant of the $(n - 1) \times (n - 1)$ matrix of $\bar{\bar{A}}$ [34]. Therefore, at the thermodynamic limit of superheat

$$\begin{vmatrix} F_{vv} & F_{vn_1} & \cdots & F_{vn_{n-1}} \\ F_{vn_1} & F_{n_1n_1} & \cdots & F_{n_1n_{n-1}} \\ \vdots & & & \\ F_{vn_n} & F_{n_1n_n} & \cdots & F_{n_{n-1}n_{n-1}} \end{vmatrix} = 0 \tag{19}$$

To illustrate, for a pure substance F(T, V, n). Along an isotherm, Equation 19 yields

$$F_{vv} = -\left.\frac{\partial P}{\partial V}\right|_{T,n} = 0 \tag{20}$$

For a binary mixture, $F(T, V, n_1, n_2)$. From Equation 19 the thermodynamic limit of superheat is defined by

$$F_{vv}F_{n_1n_1} - F_{vn_1}^2 = 0 \tag{21}$$

with

$$F_{vv} = \left.\frac{\partial P}{\partial V}\right|_{T,n_1,n_2} > 0$$

Equation 21 may be cast in a more useful form by using the definition of an ideal gas limit where $V \to \infty$ and

$$\mu_1 = \mu_1^o(T) + RT \ln \frac{n_1 \mathscr{R} T}{V} + \int_\infty^v \left.\frac{\partial \mu_1}{\partial V}\right|_{T,n_1,n_2} dV \tag{22}$$

Combining Equations 14 and 22, performing the indicated differentiations in Equation 21, and taking $n = n_1 + n_2 = 1$ yields

$$\left\{\int_v^\infty \left.\frac{\partial^2 P}{\partial n_1^2}\right|_{T,V,n_2} \cdot dV + \frac{\mathscr{R} T}{x_1}\right\} \cdot \left.\frac{\partial P}{\partial V}\right|_{T,n_1,n_2} + \left[\left.\frac{\partial P}{\partial n_1}\right|_{T,V,n_2}\right]^2 = 0 \tag{23}$$

This procedure may be extended to higher order mixtures using the Legendre transform theory [36].

The loci of states defined by Equation 19 in the general case (Equation 20 for a pure substance or Equation 23 for a binary mixture) defines the so-called "spinodal" curve of a substance. The characteristic form of this curve for a pure substance is shown in Figure 2B. Thermodynamic states outside the domain of unstable states defined by the spinodal curve are theoretically accessible.

States on the spinodal curve define the deepest possible transgression of the normal-phase boundary a liquid droplet can sustain before it must change phase. Prediction of these states requires a pressure-explicit equation of state applicable in the metastable region. Unfortunately, no such equation of state currently exists (except possibly for water [37]). One is then forced to rather arbitrarily extrapolate existing equations of state into the region of metastable states; there is a paucity of physical property data for superheated liquids. This fact puts a limitation on the ability to predict the thermodynamic limit of superheat.

For example consider the simple van der Waals equation of state for a pure substance,

$$\left(P + \frac{a}{V^2}\right)(V - b) = \mathscr{R} T \tag{24}$$

where a and b are constants (determined from the critical point definition, Equation 12a). This equation is known to inaccurately represent the saturation state of most substances. It will, however, serve a useful purpose in the present discussion. The spinodal curve (Equation 20) for the van der Waals equation of state is

$$P = \frac{a}{V^2} - \frac{2ab}{V^3} \tag{25}$$

Given a pressure P, V may be eliminated between Equations 24 and 25 to yield the thermodynamic limit of superheat, $T \to T_t$. This procedure generally requires an iterative solution (except when $P \to 0$ in which case Equations 24 and 25 yield $T = \frac{27}{32} T_c$ [38]). A simple correlation of T_t corresponding to Equations 24 and 25 which obviates this iterative procedure is [39]

$$T_t \simeq T_c \left[\frac{27}{32} + \frac{5}{32} \cdot \left(\frac{T_s}{T_c}\right)^{5.16}\right] \tag{26}$$

Table 1 lists the thermodynamic limit of superheat for six pure substances at 0.101 MPa calculated from Equation 26 (T_t). These temperatures are substantially above the normal boiling points of

Table 1
Thermodynamic Limit of Superheat of Some Pure Liquids at Atmospheric Pressure

Substance	T_s	T_{t_1}	T_{t_2}	T_m	T_c	$J(T_{t_2})$
n-pentane	309	405	431	426	470	8×10^{24}
n-heptane	372	468	499	494	540	8×10^{26}
n-octane	399	494	525	514	569	2×10^{26}
methanol	338	442	477	466	513	10^{29}
ethanol	352	447	482	472	516	10^{30}
water	373	552	596	575	647	9×10^{28}

T_s—Normal boiling point (K) at 0.101 MPa.
T_{t_1}—Calculated thermodynamic limit of superheat (K) at 0.101 MPa using the van der Waals equation of state.
T_{t_2}—Calculated thermodynamic limit of superheat (K) at 0.101 MPa using the Peng-Robinson equation of state.
T_m—Highest measured liquid phase temperature (K) at 0.101 MPa [64].
J—Nucleation rate (nuclei/cm^3-s) at T_{t_2} and .101 MPa.

the respective liquids, thus indicating that in principle the liquid phase could sustain significant superheating. This is confirmed by experiment. However, the spinodal curve is a second-law defined limit. The best experiments may thus be expected to yield maximum temperatures (or minimum pressures) such that

$$T_t(P_o) > T_m(P_o) \tag{27}$$

(rather like the inability to precisely reach 0 K). Calculated values using the van der Waals limit must therefore be rejected because measured superheat limits would then fall in the region of unstable states and thus constitute a violation of the second law. A different result is obtained if the Peng-Robinson equation of state is used to predict the thermodynamic limit of superheat. This equation [40],

$$P = \frac{\mathscr{R}T}{(v - b)} - \frac{a}{v^2 + 2bv - b^2} \tag{28}$$

(a and b are constants and v is molar volume) yields for the spinodal curve (Equation 20)

$$\frac{\mathscr{R}T}{(v - b)^2} - \frac{2a(v + b)}{(v^2 + 2bv - b^2)^2} = 0 \tag{29}$$

Equation 27 is now satisfied as shown in Table 1. However, using another equation of state would yield yet a third value of T_t. This fact illustrates a dilemma one faces when attempting to calculate the thermodynamic limit of superheat.

The situation for mixtures is even more tenuous owing to increased difficulty in accurately representing mixture properties. Figure 4 illustrates the variation of thermodynamic limit of superheat with mole fraction at 0.101 MPa for ethane/n-propane mixtures [41] using the Peng-Robinson equation of state in Equation 23. Results reveal the expected over-prediction of measurement. In view of the somewhat arbitrary value of predicted mixture thermodynamic superheat limits (different equations of state yield different predictions), it is not known if the dashed line in Figure 4 actually constitutes a true upper boundary of measured limits of superheat.

Assuming T_t predicted from the Peng-Robinson equation of state yields correct values (a tenuous assumption), differences between T_t and T_m are outside the range of the experimental uncertainty of the measurements reported in Table 1 and Figure 4. The approach to the thermodynamic

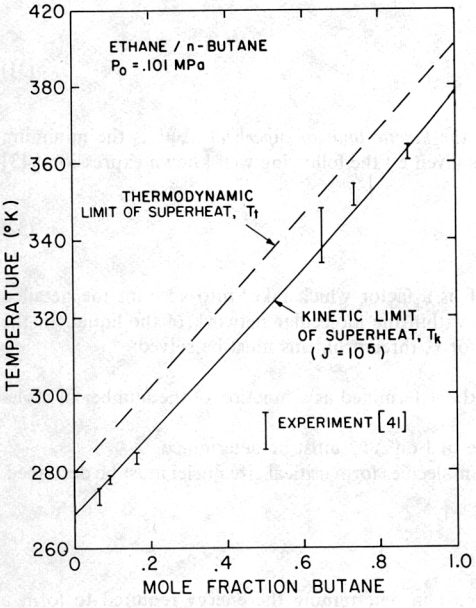

Figure 4. Comparison between highest measured liquid state temperatures (T_k) for various ethane/propane mixtures [41] and thermodynamic limits of superheat (T_t) calculated using the Peng-Robinson equation of state at 0.101 MPa.

limit of superheat then evidently triggers other phenomenon within the liquid whereby the liquid becomes "aware" of an impending violation of the second law. This conjecture forms the foundation for a mechanistic viewpoint of a phase transition which yields a practical upper limit on the superheat a liquid droplet can sustain. This mechanism defines the initial, realizable, condition for bubble growth within a droplet.

Kinetic Limit of Superheat

Introduction

A superheated liquid droplet (indeed any macroscopic liquid mass) is not quiescent on the microscopic level. Incessant random molecular motion creates local density variations. These density fluctuations in turn create "holes" or "nuclei" within which the molecules may be gas like in terms of their molecular spacing and potential energy. These nuclei grow or decay by the acquisition or loss of individual molecules until a certain size nucleus is produced such that it is in unstable equilibrium with the surrounding liquid. These bubbles are known as critical size nuclei: their appearance defines the initial condition for bubble growth within a liquid droplet.

Homogeneous nucleation theory provides a means for predicting the rate of formation of critical size nuclei at a given temperature, pressure, and composition. The mean rate of forming nuclei which continue to grow to macroscopic size is called the nucleation rate (units of nuclei/volume-time or nuclei/area-time for nucleation within the bulk of a liquid or at a surface, respectively.)

Kinetic theory [42] provides a mechanistic viewpoint for critical nucleus formation. From this theory the steady-state nucleation rate is proportional to the exponential of the energy of forming the nucleus:

$$J = \Gamma k_{f(n^*)} N_o \exp\left[-\frac{\Delta\Phi^*}{KT}\right] \tag{30}$$

or in terms of T

$$T \equiv T_k = \frac{\Delta\Phi^*}{K}\left[\ln\left(\frac{\Gamma k_{f(n^*)} N_o}{J}\right)\right]^{-1} \tag{31}$$

The temperature T_k in Equation 31 is called the *kinetic limit of superheat*. $\Delta\Phi^*$ is the minimum energy of forming a critical size nucleus and is given by the following well-known expression [43]

$$\Delta\Phi^* = \frac{16\pi\sigma_1^3}{3(P^* - P_o)^2} \tag{32}$$

where P^* is given by Equation 6 ($P \rightarrow P^*$). Γ is a factor which takes into account the detailed mechanism by which critical size nuclei form within the molecular network of the liquid. In the process of determining an explicit expression for Γ, three problems must be solved:

1. The energy of a nucleus of any size must be determined as a function of the number of molecules it contains.
2. The origin of the exponential dependence of J on $\Delta\Phi^*$ must be determined.
3. The mechanism by which the component molecules form critical size nuclei must be described.

Thermodynamics of Bubble Formation

The following assumptions are made to assist in determining the energy required to form a bubble within a superheated liquid droplet:

1. The temperature and pressure of the droplet in which the bubble forms is constant and uniform.
2. The bubble is bulk-like in terms of its thermophysical properties.
3. The bubble does not rotate, translate, or vibrate.
4. The gas within the bubble is ideal.

The so-called "capillarity approximation" which constitutes the second assumption is justified on the grounds that experimentally measured properties at the high liquid superheats typical of those characteristic of homogeneous nucleation (i.e., $T_r \gtrsim 0.9$ at $P_r > 0.04$) are in excellent agreement with predicted bulk values [44, 45].

The minimum work to form a nucleus within a homogeneous liquid under pressure P_o and temperature T is equal to the change in availability $\Delta\Phi$:

$$W = -\Delta\Phi$$

where in general [46]

$$\Phi \equiv V(P_o - P) + \sum_i \mu_i n_i + \sigma\mathscr{S} \tag{33}$$

Consider the homogeneous liquid system shown in Figure 5A, composed of a solution of n components at pressure P_o and temperature T (essentially a droplet which, relative to the bubble, appears to be of infinite extent). From Equation 33, the availability is

$$\Phi_A = \sum_i \mu'_{i1} n_{i'} \tag{34}$$

For the system in Figure 5B which includes a vapor bubble,

$$\Phi_B = \sum_i \mu'_{i2} n'_{i2} + \sum_i \mu''_i n_i + V(P_o - P) + \sigma\mathscr{S} \tag{35}$$

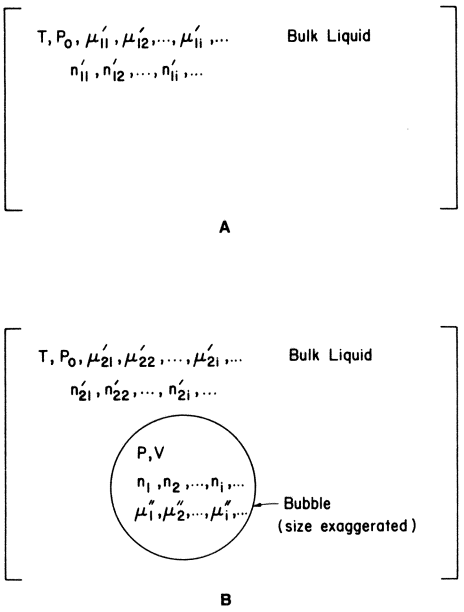

Figure 5. (A) Bulk multicomponent liquid without a vapor nucleus at indicated temperature (T), pressure (P_o), composition (n'_{ii}), and species chemical potentials (μ'_{ii}); (B) bulk liquid with vapor nucleus at indicated compositions and chemical potentials.

where n_i is the number of molecules in the vapor nucleus. Conservation of species requires that

$$n'_{i1} = n'_{i2} + n_i = \text{constant}$$

Also, since $n'_{i2} \gg n_i$ is reasonable to assume

$$\mu'_{i1} \simeq \mu'_{i2} \equiv \mu'_i(T, P_o, n'_1, n'_2, \ldots, n'_n) \tag{36}$$

Hence,

$$\Delta\Phi = \Phi_B - \Phi_A = V(P_o - P) + \sum_i n_i(\mu''_i - \mu'_i) + \sigma\mathscr{S} \tag{37}$$

In view of the ideal gas approximation, and assuming an incompressible liquid, the chemical potential difference in Equation 37 may be written as

$$\mu''_i(P_i, T) - \mu'_i(P_o, T, n'_1, n'_2, \ldots, n'_n) = KT \ln \frac{P}{P^*} + KT \ln \frac{y_i}{y_i^*} \tag{38}$$

For a spherical bubble, $V = \frac{4}{3}\pi r^3$ and $\mathscr{S} = 4\pi r^2$. Equations 37 and 38 may then be combined to give

$$\Delta\Phi = \frac{4}{3}\pi r^3\left(P_o - P + P \ln \frac{P}{p^*}\right) + 4\pi r^2\sigma + KT \sum_i n_i \ln \frac{y_i}{y_i^*} \tag{39}$$

Equation 39 is an expression for the minimum energy required to form a bubble of radius r with gas phase composition y_i in the superheated droplet.

It has been argued [47, 48] that nucleus formation will proceed in a manner which maintains the gas composition close to the value it would have at the critical size. Hence $y_i \to y_i^*$ and $P \to P^*$

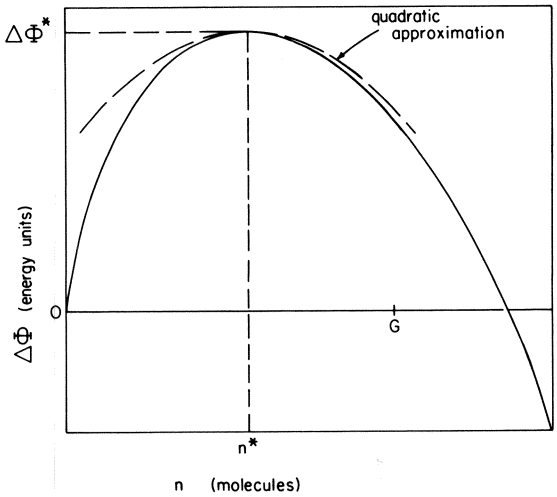

Figure 6. Typical variation of energy of forming a nucleus with number of molecules it contains. Dashed line shows representative quadratic approximation around the critical nucleus state.

(though Equation 2 will not apply for subcritical nuclei because such nuclei are not in static mechanical equilibrium). This assumption, though strictly valid only for a critical size bubble, introduces little error because its effect on the final result is only to alter the expression for Γ. In view of the ideal gas approximation

$$PV = \sum_i n_i KT \tag{40}$$

Equation 39 becomes

$$\Delta\Phi(n) = \left[36\pi\left(\frac{KT}{P^*}\right)^2\right]^{2/3} n^{2/3} - \left[KT\,\frac{P^* - P_o}{P^*}\right]n \tag{41a}$$

The qualitative variation of $\Delta\Phi$ with n is shown in Figure 6. The maximum in $\Delta\Phi$ depicted in Figure 6 defines the critical nucleus state. For this nucleus Equations 2 (with $P \rightarrow P^*$), 40, and 41 may be combined to yield Equation 32.

The stability of a critical size nucleus can be examined by twice differentiating Equation 41 ($d\Delta\Phi/dn|_{n=n^*} = 0$)

$$\Phi_{nn} \equiv \left.\frac{d^2\Delta\Phi}{dn^2}\right|_{n=n^*} = -\left(\frac{KT}{P^*}\right)^2 \frac{(P^* - P_o)^4}{32\pi\sigma^3} < 0 \tag{41b}$$

Thus, $\Delta\Phi$ does indeed exhibit a maximum at the critical size as expected. Such a nucleus is therefore in unstable equilibrium with the surrounding liquid; Equation 32 represents an effective energy barrier to bubble nucleation, and hence to bubble growth.

Kinetic Mechanism of Bubble Formation

The mechanistic view to nucleation yields a means by which nuclei may overcome the energy barrier defined by Equation 32. Among the first to propose such mechanisms were Frenkel [42], Volmer [49], and Reiss [50]. Additional theoretical work (e.g., [51–59]) has formalized the theory. Vapor nuclei are considered to grow or decay by a series of single molecule reactions. A molecule entering the nucleus results in its incremental growth; its escape causes an incremental decrease in

size (recent modifications of the classical theory accounting for nuclei-nuclei interactions are not considered here [60]).

Following the classical line of reasoning, the primitive steps in nucleus formation may be modeled by the following set of "reactions"

$$E_n + E_1 \underset{k_{r(n+1)}}{\overset{k_{f(n)}}{\rightleftarrows}} E_{n+1} \tag{42}$$

where $n = 1, 2, \ldots, n^*, \ldots, G-2$ and E_n refers to a bubble containing n molecules. There is one such reaction for each class of nucleus. The set terminates when $n > G-2$ where $G \geq n^*$ [42, 52, 53], and the reaction in the set of Equation 42 for which $n = G-1$ is irreversible. The forward and reverse "rate constants," $k_{f(n)}$ and $k_{r(n+1)}$, are molecular evaporation and condensation rates, respectively. For an ideal gas, the condensation rate is approximated by the ideal gas collision frequency,

$$k_{r(n)} = \frac{P}{\sqrt{2\pi KT}} \sum_i \frac{y_i}{\sqrt{m_i}} S_i(n) \tag{43}$$

where $S_i(n)$ is the surface area to which the species i has access for condensation, and an accommodation coefficient of unity has been assumed. The molecular evaporation rate is not known *a priori*, but may be related to $k_{r(n)}$ as discussed in the following.

The nucleation rate $I_{n,t}$ in the reaction sequence of Equation 42 is the following:

$$I_{n,t} = k_{f(n-1)} f_{n-1,t} - k_{r(n)} f_{n,t} \tag{44}$$

$f_{n,t}$ is the number of nuclei at time t in a unit volume which contain n molecules. The subscript, t, reflects the possibility that this distribution may be time dependent. A quasi-steady assumption for nucleus formation is commonly invoked. In this assumption, the time to establish a steady state nucleation rate ($I_{n,t} \rightarrow I_n$) is much shorter than the characteristic experimental time required to bring the liquid droplet into the metastable state at which the probability for formation of a critical size nucleus would be likely [59, 61]. Thus

$$\frac{\partial f_{n,t}}{\partial t} = I_{n-1,t} - I_{n,t} = 0 \tag{45}$$

Hence,

$$\cdots = I_n = I_{n+1} = \cdots = I_G \equiv J = \text{constant} \tag{46}$$

where J is the steady-state nucleation rate. This rate represents the net rate at which nuclei overcome the energy barrier to nucleation and continue to grow. This is also the rate of forming nuclei containing G molecules. For such nuclei, the corresponding reaction in the set of Equation 42 is irreversible.

The specific form of f_n is unknown. It can, however, be related to an analogous distribution conceived to exist in either

1. A superheated liquid constrained to be in hypothetical equilibrium such that $J = 0$ [e.g., 42, 52, 53].
2. In the reference normal phase equilibrium state corresponding to $r \rightarrow \infty$ [57] and $J \rightarrow 0$.

The latter approach avoids the artifice of an equilibrium distribution in a metastable liquid, while the former assumption requires some means whereby such a hypothetical equilibrium could be created. In either approach, $f \rightarrow N$ so that Equation 44 with $I = 0$ yields

$$k_{r(n+1)} = k_{f(n)} \frac{N_n}{N_{n+1}} \tag{47}$$

Equation 44 can then be written (I → J)

$$J = k_{f(n)} N_n \left[\frac{f_n}{N_n} - \frac{f_{n+1}}{N_{n+1}} \right] \tag{48}$$

Assuming that

$$f_n \to N_n \qquad \text{as } n \to 1$$

(the population of nuclei containing the smallest number of molecules is effectively the same as the equilibrium population) and

$$f_n \to 0 \qquad \text{as } n \to G$$

(there are no large nuclei present in the steady-state population), the device of summing Equation 48 from n = 1 to n = G yields

$$J = \frac{1}{\sum_{n=1}^{G-1} \frac{1}{k_{f(n)} N_n}} \tag{49}$$

The constrained equilibrium distribution, N_n, is classically determined by assuming the outwardly homogeneous superheated liquid droplet is an ideal dilute solution of vapor bubbles as solute and single molecules as solvent. On minimizing the availability of mixing such a solution it can be shown that

$$N_n \simeq N_o \exp\left[-\frac{\Delta\Phi(n)}{KT} \right] \tag{50}$$

Figure 7 illustrates the qualitative variation of N_n with n (consistent with Equation 41). Equation 50 should be regarded more as a mathematical identity than as an expression for a distribution of nuclei which could actually occur in a superheated liquid droplet. This distribution is meaning-

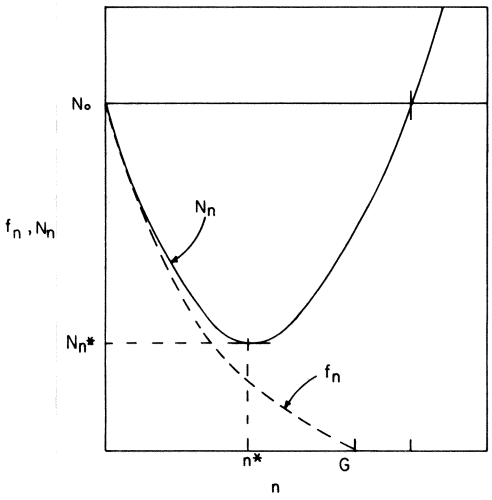

Figure 7. Schematic variation of hypothetical equilibrium (N_n) and actual (f_n) distributions of nuclei with n. Starred quantities represent the critical nucleus state.

less if n is large enough such that $N_n > N_o$. However, $f_G \to 0$ before this happens (provided G is not chosen too large).

If Equation 48 is partially summed from n = 1 to some n < G and the result combined with Equation 49, we find that

$$\frac{f_n}{N_n} < 1$$

This inequality, together with the boundary conditions on f_n, define the qualitative variation of f_n with n. This variation is shown in Figure 7. The device of summing Equation 48 [53] has obviated the need to determine a precise form of the actual distribution function f_n. Whether the equilibrium distribution is defined in the classical manner [42, 52, 53, etc.] or identified with a real distribution which exists in a saturated liquid [57] is unimportant with respect to predicting the superheat limit: differences in the two approaches will translate to minimal differences in the limiting liquid state at which a critical size nucleus is most likely to form in a liquid superheated droplet.

The present interest is in determining the thermodynamic state at which a critical size nucleus will form at the rate J in a droplet. Liquid properties appear in the distribution N_n and $k_{f(n)}$ (as yet unspecified). Equation 49 may of course be solved by iteration by including as many terms in the series as would be required to achieve a specified accuracy. This is a cumbersome approach. By treating n as a continuous rather than a discrete variable [62, 63] the summation can be converted to an integral [53]. Furthermore, the dominant contribution to this integral will occur in a region around the critical nucleus state. The consequences of this fact are two-fold:

1. A series expansion for $\Delta\Phi(n)$ truncated after the first nonzero term—a quadratic approximation (Figure 6)—is sufficiently accurate to represent the true behavior of the integral over the span of n.
2. The limits of integration may be extended from $-\infty$ to ∞ because the exponential term (Equation 50) behaves like a delta function [54]. Equation 49 then reduces to Equation 30 with

$$\Gamma = \left[\int_{-\infty}^{\infty} \exp\left[\frac{1}{2} \Phi_{nn} \cdot \frac{1}{KT} \cdot (n - n^*)^2 \right] dn \right]^{-1} \tag{51}$$

The continuous approximation for n also yields a more illuminating relation between $k_{f(n+1)}$ and $k_{f(n)}$ than given by Equation 47. In view of Equation 50 and the definition of a derivative, Equation 47 in the continuous approximation ($\Delta n = \pm 1 \to dn$ and $n \gg 1$) becomes

$$k_{f(n)} \simeq k_{r(n)} \exp\left[-\frac{\Phi_n}{KT} \right] \tag{52}$$

where $\Phi_n \equiv d\Delta\Phi/dn$. With reference to Figure 6 and Equation 41, for $n < n^*$, $\Phi_n > 0$ so that $k_{f(n)} < k_{r(n)}$. Subcritical nuclei will degenerate because of the propensity for molecular condensation over evaporation; the opposite is true when $n > n^*$ because $\Phi_n < 0$. The relative values of $k_{f(n)}$ and $k_{r(n)}$ are fundamental manifestations of the tendency for molecular transfer to or from the nuclei and can be considered a measure of the difference in chemical potential between liquid and vapor. Integrating Equation 51, noting that $k_{f(n^*)} = k_{r(n^*)}$ (Equation 52), and combining the result with Equations 42 and 43 gives

$$\Gamma k_{f(n^*)} = \left[\frac{2\sigma}{\pi} \right]^{1/2} \sum_i \frac{y_i}{\sqrt{m_i}} \tag{53}$$

(For a pure substance, $y_i \to 1$, and $m_i \to m$).

Equation 31 may now be solved for the kinetic limit of superheat, T_k (= T), given a nucleation rate. Because $\Gamma k_f N_o = 10^{35}$, a precise value of J need not be known to estimate T_k. In this respect,

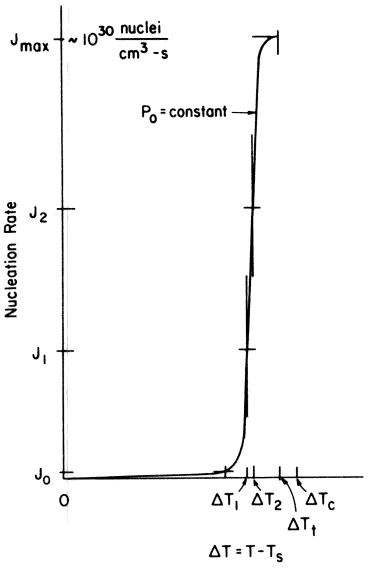

Figure 8. Variation of nucleation rate with temperature (not to scale). Peak rate ($\sim 10^{30}$ nuclei/cm^3-s) is shown corresponding to the thermodynamic limit of superheat.

T_k is a very weak function of J as schematically illustrated in Figure 8. Table 2 illustrates in numbers what Figure 8 schematically displays (using water as an example substance), and Figure 9 shows the variation of liquid temperature (Equation 31) at which critical size nuclei would form at rates J = 1, 10^5, 10^{10}, and 10^{20} nuclei/cm^3-s in n-octane (C_8H_{18}) at various pressures P_o. The range in nucleation rates shown in Figure 9 is typical of all experimental methods thus far used to measure the limit of superheat of liquids [64]. Several facts are worth noting about the kinetic limit of superheat.

The initial condition for bubble formation within a liquid droplet is not a precise value. This fact reflects the statistical nature of nucleation, yet it is usually within experimental error and thus undetectable except in the most precise measurements.

The limit of superheat increases as pressure increases. This is in agreement with experimental facts. The variation of T_k with J is not generally experimentally detectable.

Table 2
Limit of Superheat and Nucleation Rate of Water at Atmospheric Pressure

T	P	P_s	r x 10^7	J	Waiting time/cm^3 (~1/J)
500	25.8	25.2	25.2	$<10^{-99}$	$>10^{91}$ years
550	59.1	61.0	6.76	$<10^{-99}$	$<10^{91}$ years
560	68.3	71.0	5.2	1.7×10^{-76}	1.2×10^{68} years
570	78.5	82.0	3.9	8.5×10^{-20}	3.7×10^{11} years
575	83.9	88.0	3.4	5.7×10^{-3}	1.8×10^{2} sec
580	89.6	94.4	2.9	4.3×10^{9}	2.3×10^{-10} sec
590	101.6	108.9	2.1	4.3×10^{23}	2.3×10^{-24} sec

T—temperature (K)
P—pressure in vapor nucleus (atm)
P_s—equilibrium vapor pressure (atm)
r—radius of critical size nucleus (cm)
J—nucleation rate (nuclei/cm^3-sec)

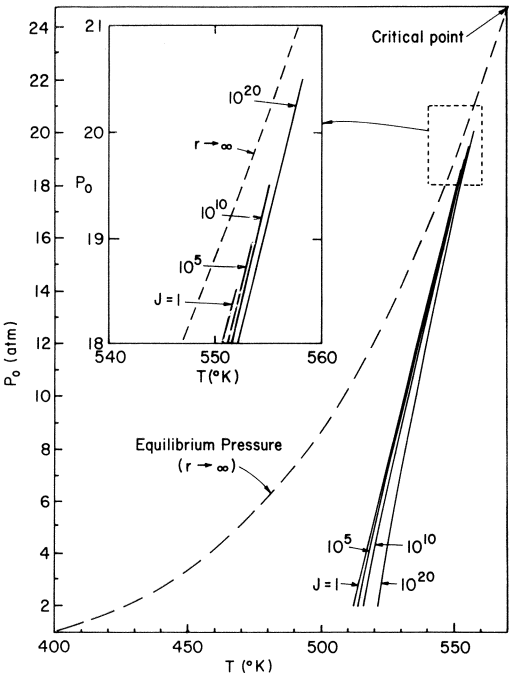

Figure 9. Calculated variation of liquid temperature with pressure at the superheat limit for n-octane corresponding to various nucleation rates. Dashed line is normal saturation curve for n-octane. Inset depicts limiting states above which no solution exists at indicated J, P_0, and T.

For constant J, the variation of T_k with P_o (solid line) appears to approach the critical point. However a solution could not be extended to the critical state while maintaining J constant in Equations 31, 32, and 53 for the n-octane properties used: $P_o \to P^*$ for some $P^* < P_c$. This fact may reflect inaccuracies in physical property prediction (most notably σ_1 and P_s) near the critical point. Another reason could be the existence of a limiting pressure above which homogeneous nucleation would not be possible at a given rate J. Above this limiting liquid pressure, $P_o > P$ and a bubble could not exist in equilibrium with a superheated liquid. This conjecture could provide a practical restriction on the ambient pressure at which a bubble could form within a superheated liquid droplet. The increasing difficulty of detecting the macroscropic manifestation of critical nucleus formation within a superheated liquid droplet (droplet vaporization) as ambient pressure is increased [29, 65] has been experimentally observed. Part of the reason for this is undoubtedly a decrease in the bubble growth rate as pressure is increased. For example, above $P_r \sim 0.75$, it is not possible to observe any outward changes of n-heptane droplets initially about 1 mm diameter in an immiscible field liquid of glycerine when the droplets are heated close to their critical point when $J < 10^{10}$ nuclei cm^3-s [29]. Calculations for several other liquids did not exhibit the limitations shown in Figure 9.

The kinetic limit of superheat at a given pressure must be lower than the thermodynamic limit of superheat. This fact creates a consistency test for calculated thermodynamic and kinetic superheat limits. Better agreement is also obtained between the kinetic superheat limit and measurement, as shown, for example in Figure 4.

Given that $T_t < T_c$ and that J increases with T_k, some range of pressures and temperatures over which the solution to Equations 31, 32, and 53 is carried must be rejected; otherwise the state so calculated would fall in the domain of unstable states (Equation 19) in Figure 2B. These boundary states imply the existence of a maximum nucleation rate for $T_s < T < T_t$ ($J \to 0$ as $T \to T_s$ and

$T \rightarrow T_c$ so that it must pass through a maximum). Table 1 lists nucleation rates at 0.101 MPa corresponding to thermodynamic superheat limits calculated from the Peng-Robinson equation of state. The orders of magnitude of J_{max} listed in Table 1 conform to values suggested in the literature [66–68] which fix this maximum at about 10^{28} to 10^{30} nuclei/cm^3-s.

Approximate Methods

The motivation for seeking approximate methods for predicting the kinetic superheat limits of liquids resides in the difficulty of accurately predicting the relevant physical properties required to solve for T_k. The most difficult property to predict, and coincidently the one on which the superheat limit exhibits the greatest sensitivity, is surface tension. (This problem is particularly severe for mixtures.) A successful method for predicting the superheat limit, and therefore the initial condition for bubble growth within a superheated liquid droplet, should obviate the need for surface tension data. A number of successful approaches have recently appeared which satisfy this intent.

One such approximation has already been presented as Equation 26 [39]. However, this approximation represents the thermodynamic limit of superheat corresponding to the van der Waals equation of state and therefore is not relevant to the present study. A more useful approach must be based on the kinetic superheat limit.

The reduced superheat limits (T/T_c) of a large number of substances have been shown to be quite close to one another at the same reduced pressure [68, 69] as illustrated in Figure 10 [68]. This fact is suggestive of a method based on corresponding states theory [70, 71]. This theory assumes that an intrinsic property of a substance, α (such as the limit of superheat corresponding to a pressure P_o and rate J), may be expressed in terms of a universal function of reduced temperature and pressure as

$$\alpha = \alpha_o(T_r, P_r)$$

Lienhard [72] recently explored this approach for the limit of superheat of pure substances by correlating reduced nucleation pressure, $P_r \equiv P/_o/P_c$, in terms of both acentric factor

$$\omega \equiv -1 - \log_{10} P_r|_{T_r = 7}$$

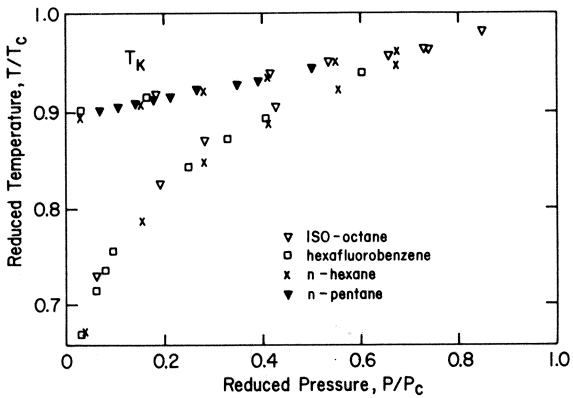

Figure 10. Reduced temperature and pressure for several substances indicating correlation of both saturation and limiting superheated liquid states [68].

and reduced superheat limit, T_r. Guided by the result from homogeneous nucleation theory, Equation 30, written in terms of pressure, is

$$P_o = P - \left(\frac{16}{3}\pi\right)^{1/2} \frac{\sigma^{3/2}}{\sqrt{kT_a}\sqrt{\ln(C/J)}} \tag{54}$$

where $T_a = T_k$ and $C = \Gamma k_{f(n^*)} N_o$. Lienhard and Karimi [66] argued the substitution of T_a by T_c, and a successful correlation was then obtained in the form [72]

$$P_{roi} = P_{rsi} - \frac{f_i}{\sqrt{-\beta}}(1 - T_{roi})^{1.83} \tag{55a}$$

where

$$f_i = 112.82 + 224.42\omega_i \tag{55b}$$

and

$$\beta = \ln(J) - C \tag{55c}$$

$$P_{roi} = P_{oi}/P_{ci}$$

$$P_{rsi} = P_{si}/P_{ci}$$

$$T_{roi} = T_{ki}/T_{ci}.$$

The term in temperature on the right-hand side of Equation 55a conforms to the classical expectation $\sigma \sim (1 - T_{roi})^{11/9}$ [71]. Fortunately C is nearly constant for a wide range of substances: $45 < C < 85$ [68, 73, 74]. The utility of Equation 55 resides both in relative accuracy and simplicity; no surface tension data are required. (In view of this accuracy, surface tension of a superheated liquid may actually be calculated by combining Equations 54 and 55 and solving for σ.) Figure 11 illustrates calculated (Equation 55) and measured superheat limits of a number of pure liquids. The data are predicted within a pencil width [72] and no surface tension data are explicitly required in the calculation.

A recent extension of the corresponding states methods for the superheat limit of a pure liquid has been made to mixtures [74]. The reduced mixture superheat limit was shown to be a mole fraction weighted average of the reduced limits of superheat of the individual components in an n-component mixture

$$T_{rm} = \sum_{i=1}^{n} x_i T_{roi} \tag{56}$$

where $T_{rm} = T_k/T_{cm}$ and the T_{roi} $(= T_{ki}/T_{ci})$ are evaluated at the same reduced pressure P_{rm} $(= P_o/P_{cm})$ as the mixture. Thus these quantities are themselves implicit functions of mole fraction through the variation of P_{cm} with x_i. The T_{ki} must be evaluated independently. This may be done by direct measurement or by using Equations 31 or 55 (depending on the availability of physical property data for the mixture in question). They are relatively constant over the range of critical pressures corresponding to $0 \leq x_i \leq 1$ at constant P_o for many substances, so the T_{ki} may be determined at only one reduced pressure and then constrained to be constants in Equation 56 over the span of x_i with little loss of accuracy [74]. The variation of T_k with x_i for the mixture is then carried entirely in T_{cm} and the explicit linear relation with the x_i. It should be noted that while the reduced superheat limits calculated from Equation 56 exhibit a linear variation with mole fraction,

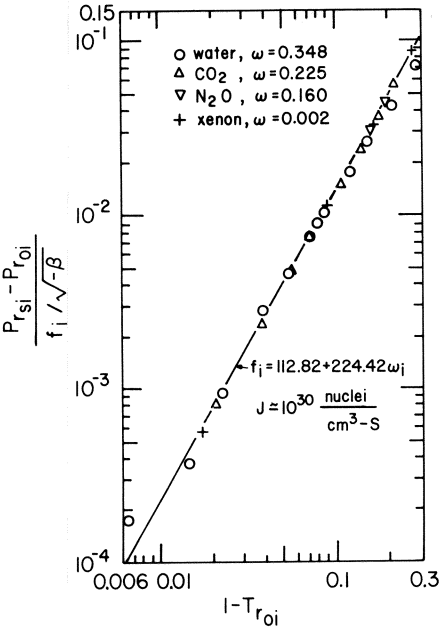

Figure 11. Corresponding states correlation of the homogeneous nucleation limits of liquids [72].

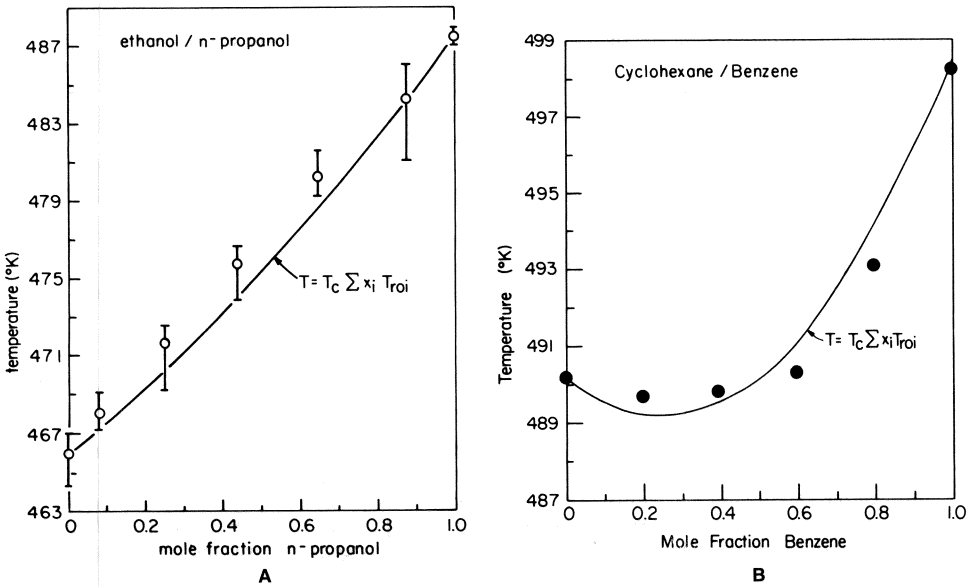

Figure 12. Comparison between measured kinetic limits of superheat of several ethanol-n -propanol (A) and cyclohexane/ benzene (B) mixtures [48] with predictions of the generalized corresponding states method at various mixture compositions [74].

the superheat limit itself will not generally vary linearly with x_i. Only when

$$T_{cm} = \sum_{i=1}^{n} x_i T_{ci}$$

and the T_{roi} are all the same over the span of x_i for constant P_o does Equation 56 yield the often quoted result

$$T_k = \sum_{i=1}^{n} x_i T_{ki} \tag{57}$$

Figures 12A and B illustrate the variation of T_k with x_i for two binary mixtures. It is evident that inaccurate predictions may generally be expected if Equation 57 is assumed to be universally valid.

Conclusions

The practically attainable superheat limit of a liquid corresponds to the kinetic limit of superheat. This limit may be either measured or predicted using the approach based on classical homogeneous nucleation theory or from one of the recent approximate corresponding states methods. Though this discussion has been in the context of liquid droplets, the results are independent of droplet volume as long as the liquid state is not appreciably altered from the ambient by the droplet/field liquid interfacial tension. In any case, the result gives the thermodynamic state—pressure, temperature, and composition—at which super-critical nuclei (the initial bubbles) form within the bulk of the droplet at a particular nucleation rate. However, merely defining the thermodynamic state for initial bubble formation does not provide information concerning the dynamics of phase change.

BUBBLE GROWTH IN DROPLETS

Introduction

Critical size nuclei are in static (unstable) equilibrium and would remain in this state unless perturbed by a change in pressure, temperature, or composition. Such a perturbation is inherent in the nucleation process itself in that the nucleation rate prescribes the rate of forming supercritical nuclei (containing $n > n^*$ molecules). These nuclei are not in static equilibrium in as much as $k_{f(G)} > k_{r(G)}$ (Equation 52). Inherent in the nucleation process is thus the further growth of supercritical nuclei. The process of homogeneous nucleation itself is considered to end with the appearance and subsequent growth of these nuclei.

As the initial bubble grows both its pressure P and temperature T_v decrease (path $2 \rightarrow 2'$ in Figure 2A). Growth continues until $P \rightarrow P_o$ and $T_v \rightarrow T_s$. Finally, when liquid 1 completely vaporizes, the final vapor bubble at T_v must be reheated to T_o to regain thermal equilibrium. These aspects of bubble growth are well documented with reference to bubbles growing in infinite media (see, for example, the excellent reviews in References 75 and 76).

The dynamics of growth within a droplet may be affected from the beginning by the finite mass of vaporizing liquid. For both small liquid/liquid interfacial tensions and differences between the two fluid densities, the initial bubble exhibits a growth similar to its growth in an infinite media ($S \rightarrow \infty$). The initially isothermal field within the droplet is perturbed due to expansion of the bubble. A thermal boundary layer is created at the evaporating boundary which may initially be far removed from the boundary of the droplet (depending, of course, on the physical location of the initial bubble in the droplet; regardless of this location there will be *some* period of growth. that is, the boundary layer does not penetrate into the field liquid). Figure 13 illustrates the qualitative picture. As the bubble grows and its temperature continues to drop, the thermal boundary layer propagates progressively farther into the vaporizing liquid and eventually reaches the droplet

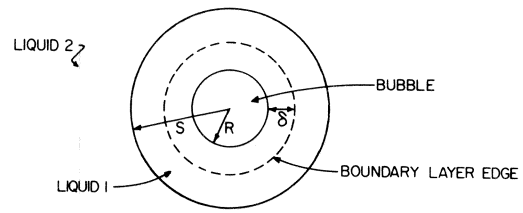

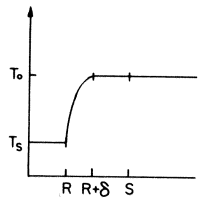

BOUNDARY LAYER INSIDE DROPLET

A

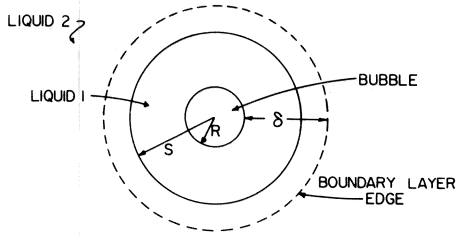

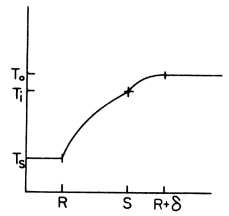

BOUNDARY LAYER OUTSIDE DROPLET

B

Figure 13. Schematic illustration of bubble growth in a droplet suspended in an immiscible liquid: (A) early stage where thermal boundary layer (δ) is within the droplet; (B) later stage where boundary layer extends into liquid 2.

boundary (Figure 13B). Until that time growth will be very similar to that which would occur in an infinite medium, as the temperature field in liquid 2 remains unperturbed. The conservation equations governing bubble growth in a droplet will then be identical to those for bubble growth in an infinite media. When the thermal boundary layer extends into liquid 2 the temperature and pressure fields in both liquids must be determined at each instant of time, as well as the radial history of the bubble.

Review of Bubble Growth in Stationary Infinite Media

Governing Equations

Consider an isolated bubble expanding in a pure inviscid constant property uniformly superheated liquid at temperature T_o and pressure P_o. We shall utilize all assumptions made in an earlier study of this problem [77]. Viscous effects are also neglected [76]. For a stationary spherical bubble growing in a stagnant inviscid liquid the velocity field is [77, 78]

$$v = \varepsilon \frac{R^2}{r^2} \dot{R} \tag{58}$$

where $\varepsilon = 1 - \rho_v/\rho_1$. When Equation 58 is combined with the inviscid momentum equation,

$$\frac{D\bar{v}_i}{Dt} = -\frac{1}{\rho_i} \bar{\nabla} P_i \tag{59}$$

(where i = 1 denotes the droplet and i = 2 is the immiscible field liquid) and integrated

$$\int_R^S \left\{ \frac{\varepsilon}{r^2} [\ddot{R}R^2 + 2\dot{R}^2 R] - 2\varepsilon \frac{R^2 R^4}{r^3} \right\} dr = -\frac{1}{\rho_i} \int_R^S dP_i \tag{60}$$

the classical Rayleigh equation emerges when $S \to \infty$ and Equation 2 is used to replace interfacial pressure in the liquid with surface tension and radius [76, 77, 79]:

$$R\ddot{R} + \dot{R}^2 \left(2 - \frac{\varepsilon}{2} \right) = \frac{P - P_o}{\varepsilon \rho_1} - \frac{2\sigma_1}{\varepsilon \rho_1 R} \tag{61}$$

The energy equation governing the temperature field in liquid 1 (which is effectively infinite during the time for which $\delta < S - R$) is

$$\frac{\partial T_i}{\partial t} + \vec{v}_i \cdot \bar{\nabla} T_i = \alpha_i \bar{\nabla}^2 T_i \tag{62}$$

(where i = 1). The boundary and initial conditions are the following:

$r = R$: $$T_1 = T_v(t) \tag{63a}$$

$$k_1 \left. \frac{\partial T_1}{\partial r} \right|_{r=R} = \rho_v h_{fg} \dot{R} \tag{63b}$$

$r \to \infty$: $$T_1 \to T_o \tag{63c}$$

$t = 0$: $$T_1 = T_o \tag{63d}$$

$$R = R_o \tag{63e}$$

$$\dot{R} = 0 \tag{63f}$$

The phase equilibrium condition which couples Equations 61–63, neglecting nonequilibrium effects [80, 81], is

$$P = P(T_v(t)) \tag{63g}$$

The specific form of this relation depends on the fluid under consideration. In general the often used linearized Clausius/Clapeyron equation (e.g., [82, 83])

$$P[T_v(t)] \simeq P_o + \rho_1 \mathscr{A}[T_v(t) - T_s(P_o)] \tag{64}$$

where $\mathscr{A}$ is a constant dependent on the specific fluid, will not generally be accurate at the high liquid superheats of interest here ($T_o - T_s > 100$ K at $P_r \sim 0.04$) except when $P_r \to 1$.

The unknowns in Equations 61–63 are $T_1(r, t)$, $P(t)$, $T_v(t)$, and $R(t)$. A rather large number of solutions to this set of equations has appeared in the literature, which range from approximate analytical solutions to fully numerical treatments that involve no further approximations than are already incorporated in the governing equations as written. These solutions may be divided into three classes:

1. Solutions in which only the momentum equation (Equation 61) is solved.
2. Solutions in which the full set of Equations 61–63 is solved simultaneously.
3. Solutions for which only the energy equation is solved.

Approximate Solutions

Inertia controlled growth. The initial temperature field is isothermal so that growth is controlled by the difference in pressure which exists across the liquid/vapor interface ($\Delta P \equiv P - P_o$). This pressure difference may be large for a droplet at its superheat limit. For example, for critical size nuclei $R_o \sim 10^{-7}$ cm and $\sigma \sim 3$ dyne/cm (typical of many organic liquids at $T_r \sim 0.9$). Therefore, $\Delta P \sim$ (10 atm).

The solution of Equation 61 yields a bubble growth rate in the form

$$\dot{R} = C_1$$

where [76, 79, 83, 84]

$$C_1 = \left\{\frac{2}{3}\frac{P - P_o}{\varepsilon\rho_1}\left[1 - \left(\frac{R_o}{R}\right)^3\right] - \frac{2\sigma_1}{\varepsilon\rho_1 R}\left[1 - \left(\frac{R_o}{R}\right)^2\right]\right\}^{1/2} \tag{65a}$$

When $R \gg R_o$ and the surface tension term is neglected, C_1 becomes independent of R such that

$$C_1 \simeq \left\{\frac{2}{3}\frac{P - P_o}{\varepsilon\rho_1}\right\}^{1/2} \tag{65b}$$

The evolution of bubble radius then takes the form

$$R \simeq C_1 t^q \tag{66}$$

where $q = 1$.

Immediately after the bubble starts to expand, the gas pressure as well as both the gas temperature and temperature of the liquid adjacent to the bubble wall begin to drop. Eventually, $T_v \to T_s$ and $P \to P_o$ (though in fact ΔP is never identically zero). The temperature gradient at the bubble wall then controls growth (Equation 63b) and this gradient is determined by solving the energy equation (Equation 62); the momentum equation is not now needed.

Heat transfer controlled growth. Various analytical solutions to Equations 62 and 63b yield a bubble growth law of the same form as Equation 66 with

$$q = \tfrac{1}{2} \tag{67}$$

[77, 83–86]. The solutions differ in the growth constant C_1. Scriven [77] discovered a similarity variable for Equation 62 and showed that C_1 is obtained by numerically solving

$$\mathrm{Ja} = 2\beta^3 \exp[\beta^2 + 2\varepsilon\beta^2] \int_\beta^\infty X^{-2} \exp[-X^2 - 2\varepsilon\beta^3 X^{-1}]\, dX \tag{68}$$

where the Jakob number is defined as

$$\mathrm{Ja} = \frac{\rho_l C_{pl}(T_o - T_s)}{\rho_v h_{fg}} \tag{69}$$

and

$$\beta = \frac{C_1}{2\alpha_l^{1/2}} \tag{70}$$

(The Jakob number has also been found to be an important parameter for defining the intensity of vaporization of droplets [27].) Birkhoff et al. [86] used the same similarity variable as Scriven and arrived at a similar result.

Approximate solutions to Equation 62 were obtained by Plesset and Zwick [83] and Forster and Zuber [85] in the form

$$C_1 = \mathrm{Ja} \cdot (C\alpha_l)^{1/2} \tag{71a}$$

where

$$C = \pi[85] \tag{71b}$$

or

$$C = \frac{12}{\pi}[84] \tag{71c}$$

Plesset and Zwick employed the assumption of a "thin" thermal boundary layer in their analysis. This assumption requires that $\mathrm{Ja} \gg 1$ [76]. At lower superheats wherein this approximation is no longer valid, the growth constant must be determined by numerically solving Equations 68–70.

An approximate analytical expression for C_1 was presented by Moalem-Maron and Zijl [87] (for $R \gg R_o$) which agrees with the limiting values for small ($\mathrm{Ja} \ll 1$) [77] and large ($\mathrm{Ja} \gg 1$) [77, 83] Jakob number:

$$C_1 \simeq \left(\frac{3\alpha_l}{\pi}\right)^{1/2} \mathrm{Ja}\left\{1 + \sqrt{1 + \frac{2\pi}{3\mathrm{Ja}}}\right\} \tag{72}$$

The growth law expressed by Equation 66 with $q = \frac{1}{2}$ exhibits a singularity as $t \to 0$. This fact does not usually cause difficulties. When fluid conditions are such as to render valid the assumption of heat-transfer-controlled growth, the size range of visible bubbles is usually large enough that this initial velocity singularity has a minimal effect on predicted bubble radii.

Growth in the intermediate region. The full set of equations (Equations 61–63) must be solved when the already mentioned asymptotic approximations are not valid. There is no closed-form analytical solution to this set of equations. Either fully numerical procedures [88–90] or approximate analytical/numerical methods must be used (e.g., [83, 85, 91, 92]). A review of some of these solutions is given in Reference 76.

The simplest of the approximate solutions and one which also yields limits of validity of the asymptotic solutions previously discussed was obtained by Mikic et al. [82] and later modified by

Theofanous and Patel [93]. Their approach was to solve the asymptotic expressions for bubble growth given by Equation 66 with q = 1 (Equation 65b) and q = $\frac{1}{2}$ (Equation 71c) for $T_v(t)$, and then eliminate $T_v(t)$ between the two equations. Only small superheats were considered such that $(T_v - T_s)/(T_o - T_s) \sim 1$ and the linearized Clausius-Clapeyron equation was used to replace P by $T_v(t)$ in Equation 65b. The result was the following:

$$R^+ = \tfrac{2}{3}[(t^+ + 1)^{3/2} - t^{+3/2} - 1] \tag{73a}$$

where

$$R^+ = \frac{A}{C_1^2} R \tag{73b}$$

$$t^+ = \frac{A^2}{C_1^2} t \tag{73c}$$

$$A = \left(\frac{2}{3} \frac{h_{fg}\rho_v(T_o - T_s)}{\rho_1 T_s}\right)^{1/2} \tag{73d}$$

The utility of Equation 73 lies in its simplicity. It facilitates calculating the temporal variation of R which spans the range of controlling mechanisms for bubble growth.

The real time domain over which the approximate asymptotic solutions thus far considered may be valid can be estimated from Equation 73. When $t^+ \ll 1$, Equation 73 yields the correct limit for inertia controlled bubble growth, while for $t^+ \gg 1$, the correct limit for heat-transfer-controlled growth is recovered. At the superheat limit corresponding to $P_r \sim 0.04$ for many organic liquids, $200 < Ja < 300$ (Figure 14) which, unfortunately, is outside the range of validity of Equation 73a. We only intend to use Equation 73 here to establish approximate limits for the validity of the various asymptotic solutions. The order of magnitude of relevant properties of many organic liquids at $T_r \sim 0.9$ is the following: $Ja \sim 10^2$, $h_{fg} \sim 10^3$ cal/g, $\alpha_1 \sim 10^{-4}$ cm^2/s, $T_s \sim 10^2$ K, $\Delta T \sim 10^2$ K, $\rho_1 \sim 0.1$ g/cm^3, and $\rho_v \sim 10^{-2}$ g/cm^3. From Equation 73c $t^+ \sim 10^3 t$. The temperature field will then essentially be isothermal for times $t \ll 1$ ms. As pressure increases, Ja decreases (Figure 14) and the time domain for isothermal growth becomes progressively shorter.

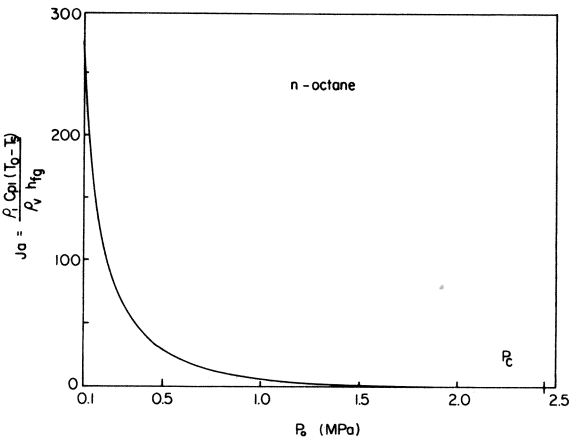

Figure 14. Typical variation of Jakob number (Ja) with pressure (P_0) at its superheat limit using properties of n-octane for illustration.

Experimentally accessible times for bubble growth measurements within superheated liquid droplets have, with one exception [18], been on the order of 1 ms [11, 27, 28]. The available data are thus representative of phase change dominated by heat transfer processes.

Bubble Growth in Finite Media—Droplets

Introduction

The application of an analysis for bubble growth in an infinite medium to growth in a liquid of finite extent (i.e., a droplet) requires that the thermal boundary layer does not penetrate into the region outside of the droplet boundary (Figure 13A). As the bubble grows and the droplet evaporates, the bubble wall approaches the liquid/liquid interface, and clearly the thermal boundary layer must eventually extend into the field liquid (Figure 13B). In this event, the temperature field is a two-domain problem and the full set of Equations 61–63 must be solved simultaneously to determine the temporal variation R, T_v, P, and S. A number of solutions to this set of equations have been obtained which involve various approximations which we shall review here. As a prelude, we first provide criteria which will ensure that the initial bubble forms within the bulk of the droplet and not at the liquid 1/liquid 2 interface. Then we shall define an appropriate geometrical configuration for the two-phase droplet.

The liquid 1/liquid 2 interface represents an ideal smooth container for a droplet. The process of homogeneous nucleation may equally occur at this interface as in the bulk of the droplet. The relative value of the nucleation rate determines the location of bubble formation, with nuclei forming in the region where J is highest. For most purposes, this requirement is equivalent to determining where $\Delta\Phi$ (Equation 32) is lowest. Exceptions are sometimes encountered for nuclei forming at solid surfaces [94]. Five possible locations for nuclei formation may be identified (Figure 15):

1. Completely within the bulk of the droplet (position 1).
2. At the liquid 1/liquid 2 interface but resting entirely within liquid 1 (position 2 in Figure 15):
3. Between liquid 1 and liquid 2 (position 3):
4. At the liquid 1/liquid 2 interface but resting entirely within (position 4):
5. Completely within liquid 2 (position 5):

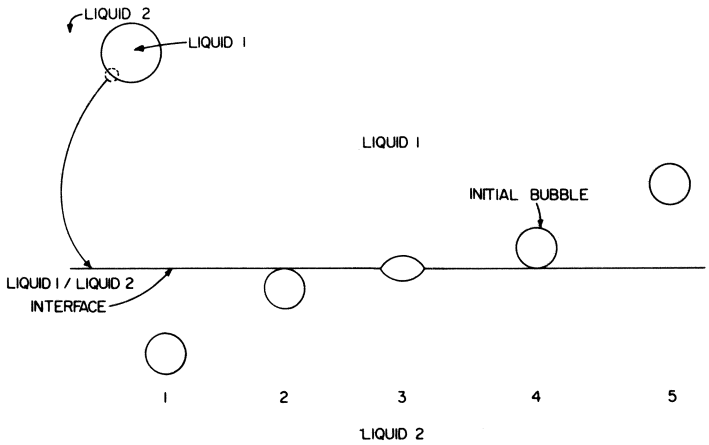

Figure 15. Possible locations of initial bubble appearance within a superheated droplet (liquid 1) relative to interface between droplet and field liquid (liquid 2).

The basis for expecting nucleation to occur at the liquid 1/liquid 2 interface is determined by the interfacial forces acting on the vapor lens (position 3) and the energy of the critical size bubble. If a lenticular nucleus (position 3) is to be stable, then we must assure that [16, 73, 95–97]

$$\sigma_{12} = |\sigma_1 - \sigma_2| \tag{74a}$$

Otherwise, if

$$\sigma_1 \geq \sigma_2 + \sigma_{12} \tag{74b}$$

or

$$\sigma_2 \geq \sigma_1 + \sigma_{12} \tag{74c}$$

the nucleus forms in the liquid with the lower surface tension. This latter possibility is of interest in the present discussion and corresponds to the tendency of liquid 1 to spread on liquid 2 [98]. The bubble will then remain within the boundaries of the droplet and liquid 2 will serve only as a medium for heating the droplet and will not itself affect the ability of the droplet to be heated to its limit of superheat. Liquid 2 will, of course, affect the bubble growth process when the thermal boundary layer penetrates into it. If Equations 74a or 74b were satisfied, a bubble might leave the droplet before all of liquid 1 vaporizes [16, 17, 24, 99]. In the present work the bubble is considered to remain entirely within the boundary of the droplet and does not penetrate the liquid 1/liquid 2 interface during its growth. The surface tension of the vaporizing liquid is then low compared to the liquid 2 surface tension and Equation 74c is satisfied.

Geometry of the Two-Phase Droplet

The spatial location of the initial bubble within an isothermal droplet will be random unless temperature gradients exist within the droplet. A simple mass balance on the droplet reveals that this initial location is unimportant during evaporation of most of the liquid mass of the droplet. A mass balance shows that the ratio of bubble radius R to droplet radius, S, is

$$\frac{R}{S} = \left[\frac{\chi}{1 - \varepsilon(1 - \chi)}\right]^{1/3} \tag{75}$$

where χ is the mass fraction of liquid evaporated. For many liquids, $\varepsilon > 0.9$ at $T_r \sim 0.9$. When as little as 10% of liquid is evaporated, $R/S \sim 0.8$; when 50% of the liquid in the droplet has evaporated, $R/S \sim 0.97$. In either case the unevaporated liquid will essentially exist as a relatively thin film around the bubble. This fact has been observed experimentally [11, 21]. Effects due to eccentricity of the vapor bubble (Figure 16A) will be minimal after this initial evaporation. The salient features of evaporation of a bubble within a droplet were therefore examined with the aid of the model shown in Figure 16B—a vapor bubble growing from the center of a liquid droplet.

Approximations and Previous Work

The equations governing bubble growth in a droplet are Equations 59, 62, and 63 with $i = 1, 2$. The problem requires solving both the momentum and energy equations simultaneously within liquids 1 and 2, taking due account of their coupling at the liquid/liquid interface. We first review here simplifications to this problem which have appeared in the literature.

Main simplifications involved neglect of detailed dynamics and heat transfer processes within the droplet. Sideman and Taitel [21] and Tochitani et al. [100] assumed the two-phase droplet was a rigid sphere to determine both the temperature field in the ambient liquid (i.e., the temperature adjusts instantaneously to changes in droplet radius) and average Nusselt number around the droplet when

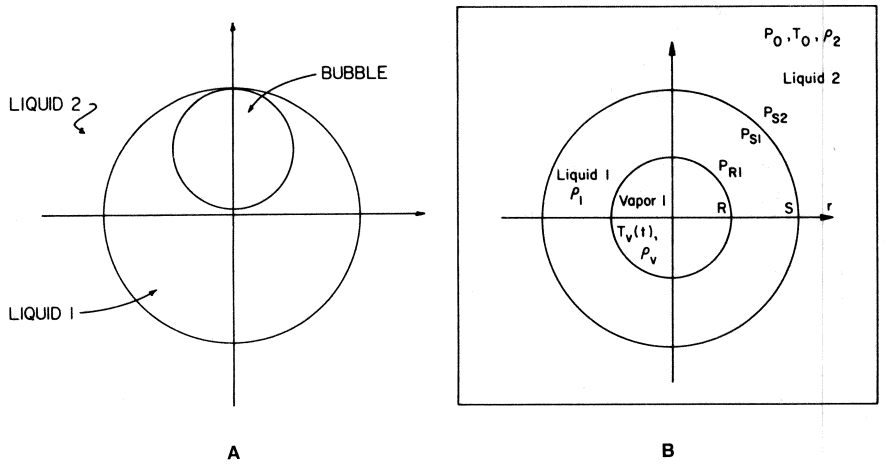

Figure 16. Geometric model for bubble growth in a liquid droplet. (A) bubble geometry as determined by photographs from several experiments; (B) simplified geometric model used in present analysis (pressures correspond to values at indicated interfaces).

heat transfer occurred over part of the surface of the droplet. The remainder of the boundary was considered insulated. Sideman and Isenberg [22] later used this Nusselt number to determine the temporal variation of droplet radius using the two-phase droplet model shown in Figure 17. A similar model was used by Moalem-Maron et al. [101] except heat transfer was accounted for over the entire surface of the droplet. Selecki and Gradon [25] extended this model to an evaporating (nonrigid) droplet and used the result for bubble growth in an infinite medium (Equation 71) to describe the temporal variation of droplet radius. Detailed account of the external flow field for both an expanding and translating droplet was included in the analysis of Mokhtarzadeh and El-Shirbini [26], while the droplet interior was considered to be at a uniform temperature with an average heat transfer coefficient used to determine heat transfer to the droplet. An analysis of bubble growth in droplets when Equation 74b is satisfied (liquid 2 now spreads on liquid 1) has also been reported such that the bubble was either considered to leave the droplet as soon as it formed [24] or after moving through the liquid 1/liquid 2 interface [99]. This latter study [99] utilized a modification of Equations 66, 67, and 71 and included vapor density variations with temperature, while the former work [24] obtained the temperature and velocity fields within the droplet only for those periods between departure of the nucleus from the droplet to its subsequent formation (i.e., for a single-phase droplet exposed to a liquid 2 in uniform motion).

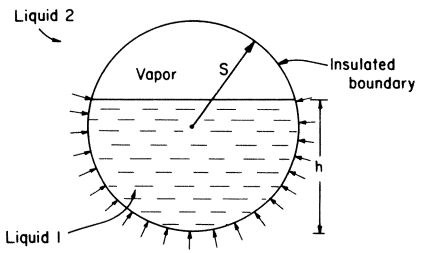

Figure 17. Model for quasi-steady vaporization of a droplet in an immiscible liquid when thermal boundary layer extends well into liquid 2 and the vapor/liquid 2 boundary is assumed insulated [22].

The solutions referred to previously employed various approximations including neglect of radial liquid motion, dominant axial convection (i.e., moving droplets), quasi-steady heat transfer, or taking full account of the transient temperature field. The importance of translatory motion resides in the fact that experimental methods often involve moving droplets. The quasi-steady approximation involves certain assumptions about the characteristic times for heat transport and bubble expansion. Delineation of the important characteristic parameters which govern these approximations will aid in both classifying the various solutions presented and in establishing the most simplified form of the equations governing bubble growth in a liquid droplet at the superheat limit. For this purpose we will initially consider an isolated expanding bubble in uniform motion in a static liquid. Whether we consider this configuration or focus attention on an internal bubble within a droplet is unimportant with regard to the present intent. The droplet may expand at about the same rate as the internal bubble during most of the evaporation. It is only desired here to estimate the standard order of magnitude of the terms in the energy equation to ascertain which terms are important and which are not.

For a translating and expanding droplet the velocity field, Equation 58, must be modified. We follow previous work and neglect viscous effects around the droplet. The velocity field is then [102, 103]

$$V_r = U_\infty \left(1 - \frac{R^3}{r^3}\right) \cos\theta + \varepsilon \frac{R^2}{r^2} \dot{R} \tag{76a}$$

$$V_\theta = U_\infty \left(1 + \frac{R^3}{2r^3}\right) \sin\theta \tag{76b}$$

where θ is measured from the vertical. Equations 62 and 76 are combined and nondimensionalized to yield

$$\underset{\text{(A)}}{\frac{\partial \bar{T}}{\partial \tau}} + \underset{\text{(B)}}{\left[\varepsilon \frac{\bar{R}^2}{\bar{r}^2} \dot{\bar{R}} - \text{Pe}\left(1 - \frac{\bar{R}^3}{\bar{r}^3}\right)\right] \frac{\partial \bar{T}}{\partial \bar{r}}} + \underset{\text{(C)}}{\text{Pe}\left(1 + \frac{\bar{R}^3}{\bar{r}^3}\right) \frac{\sin\theta}{\bar{r}} \frac{\partial \bar{T}}{\partial \bar{r}}}$$

$$= \underset{\text{(E)}}{\frac{1}{\bar{r}^2} \frac{2}{\partial \bar{r}} \left(\bar{r}^2 \frac{\partial \bar{T}}{\partial \bar{r}}\right)} + \underset{\text{(F)}}{\frac{1}{\bar{r}^2} \frac{1}{\sin\theta} \frac{\partial}{\partial \theta} \left(\sin\theta \frac{\partial \bar{T}}{\partial \theta}\right)} \tag{77}$$

where the Peclet number is defined as

$$\text{Pe} = \frac{U_\infty S_o}{\alpha_1} \tag{78a}$$

$$\tau = \frac{\alpha_1 t}{S_o^2} \tag{78b}$$

$$\bar{T} = \frac{T - T_s}{T_o - T_s} \tag{78c}$$

$$\bar{r}, \bar{R} = r, R/S_o \tag{78d}$$

The boundary conditions are approximately given by Equation 63. Translational convection (terms (C) and (D)) may be neglected in comparison with radial convection (B) if

$$\text{Pe} \ll \frac{\text{Ja}}{\bar{\delta}^2} \tag{79}$$

where from Equation 63b, $\bar{\dot{R}} \sim Ja/\bar{\delta}$ has been used; $\bar{\delta}$ is the nondimensional boundary layer thickness ($= \delta/R$). Now, in analogy with bubble growth in an infinite medium, $\bar{\delta}$ is approximated as [76]

$$\bar{\delta} \sim 1/Ja \tag{80}$$

Equation 79 is then

$$Pe \ll Ja^3 \tag{81}$$

On the other hand if

$$Pe \gg Ja^3 \tag{82}$$

translational convection dominates.

The validity of the quasi-steady approximation resides in the relative values of characteristic time for thermal diffusion in the liquid surrounding the bubble, and the characteristic bubble expansion time. If Equation 81 is satisfied the characteristic time for heat diffusion in the liquid surrounding the bubble is

$$t_H \sim \frac{R^2}{\alpha_1} \tag{83a}$$

If radial convection is of negligible importance and translational motion of the droplet dominates (Equation 82), then approximately

$$t_H \sim \frac{R}{U_\infty} \tag{83b}$$

In either case, the characteristic bubble expansion time is estimated from Equations 63b ($\partial T/\partial r \sim \Delta T/\delta$) and 80 as

$$t_R \sim \frac{R^2}{\alpha_l Ja^2} \tag{84}$$

When Equation 82 applies,

$$\frac{t_R}{t_H} \sim \frac{Pe}{Ja^2} \gg 1 \tag{85a}$$

so unsteady heat transfer in the liquid surrounding the bubble may also be neglected (i.e., the time-dependent term in Equation 62 may be dropped and the quasi-steady approximation is reasonable). When radial motion dominates (in the limit, $Pe \to 0$)

$$\frac{t_R}{t_H} \sim \frac{1}{Ja^2} \tag{85b}$$

The quasi-steady approximation will then be reasonable only for low Jakob number. For many liquids heated to their superheat limits, $Ja \sim \theta(10^2)$ at $P_r \sim 0.04$ (Figure 14). The quasi-steady approximation is then not valid as the thermal boundary layer remains close to the bubble. The time-dependent term in Equation 62 must be retained in the solution. When $T_r \to 1$ ($P_r \to 1$ in view of the fact that the limit of superheat is not independent of pressure) $Ja \to 0$ and the thermal boundary layer is thick relative to the droplet radius. Liquid phase quasi-steadiness may then be assumed.

(Near the critical pressure, though, gas phase unsteadiness becomes increasingly important to consider.) The fact that this approximation has been used at much lower superheats in previous work (e.g., [104]) is indicative of extraneous nucleation aids suppressing homogeneous nucleation.

Quasi-Steady Solutions

The quasi-steady approximation has led to a number of approximate analytical solutions for the temporal variation of droplet radius, which do not involve the equation of motion. In the extreme case of negligible radial convection (Equation 82) the droplet is considered a rigid sphere and viscous effects are neglected. Sideman and Taitel [21] and Sideman and Isenberg [22] considered a two-phase droplet to be a spherical shell of vapor with a puddle of liquid at the bottom (Figure 18A). Heat transfer over the upper portion of the droplet—the liquid 2/vapor interface—was neglected. The average Nusselt number characterizing heat transfer to the liquid sheath in a potential flow field was obtained as [21]

$$\mathrm{Nu} = \frac{h \cdot 2R}{k_1} = 2\left(\frac{\mathrm{Pe}}{\pi} \cdot \left[\frac{1-(1-\varepsilon)\bar{S}^3}{\varepsilon \bar{S}^4}\right]\right)^{1/2} \tag{86}$$

where $\bar{S} \equiv S/S_o$. Using Equation 86 in an energy balance at the liquid 1/liquid 2 interface, $\bar{S}$ was determined as [22]

$$\bar{S} = (1-\varepsilon)^{-1/3}\left\{1-\varepsilon\left[\left(\frac{9}{2\pi}\right)^{1/2}(1-\varepsilon)\mathrm{JaPe}^{1/2}\tau - 1\right]^2\right\}^{1/3} \tag{87}$$

The variations of $\bar{S}$ with τ is shown in Figure 18 for one particular set of conditions corresponding to pentane droplets in water with Pe = 5,000, Ja = 4.3, $\Delta T = 5°K$, and $S_o = 1.5$ mm [22]. Conditions of their data were such that the origin of the initial bubble was not homogeneous nucleation, but extraneous nucleation aids of the type not of principle interest here: deliberately introduced air bubbles or solid particles. The corresponding superheats were far lower than values characteristic of homogeneous nucleation.

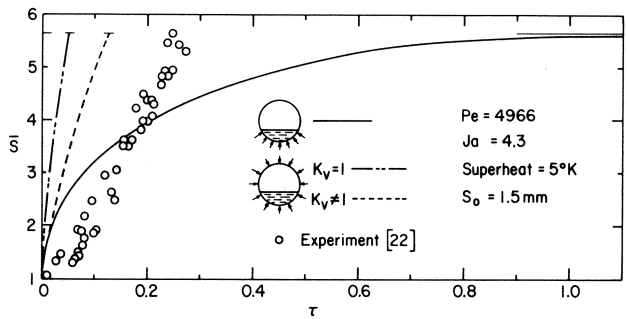

Figure 18. Comparison between predicted and observed droplet radii at various times (τ) and low superheats. Data from Reference 22 and simplified analyses from References 22 (Equation 87) and 101 (Equation 91).

Viscous effects in the flow field around the droplet were accounted for in an ad-hoc manner by Moalem-Maron et al. [101]. The viscous flow Nusselt number around a rigid sphere

$$\mathrm{Nu} = \frac{2}{\pi^{1/2}}(0.25\mathrm{Pr}^{-1/3}\mathrm{Pe})^{1/2} \tag{88}$$

was written in a form analogous to the potential flow solution,

$$\mathrm{Nu} = \frac{2}{\pi^{1/2}}\mathrm{Pe}^{1/2}$$

by defining [101, 105]

$$k_v = 0.25\mathrm{Pe}^{-1/3} \tag{89}$$

k_v was considered a correction by which the inviscid flow solution around a rigid sphere would be transformed to yield the average heat flux around an expanding sphere in a viscous flow field. Hence,

$$\mathrm{Nu} \simeq 2\left(\frac{\mathrm{Pe}}{\pi}k_v\right)^{1/2} \tag{90}$$

Considering heat transfer to occur over the entire surface of the droplet (a more reasonable assumption when liquid 1 spreads on liquid 2), a heat balance yielded

$$\bar{S} = \left[1 + \frac{3}{2}\mathrm{Ja}\frac{\zeta}{\gamma}\mathrm{Pe}^{1/2}\left(\frac{k_v}{\pi}\right)^{1/2}\tau\right]^{2/3} \tag{91}$$

Figure 18 illustrates the variation of $\bar{S}$ with τ for the same approximate set of conditions as reported by Sideman and Isenberg [22].

Dominant Radial Convection

Equations. All experimental methods used to create superheated liquid droplets involved slowly moving droplets. With characteristic velocities of all methods on the order of $U_\infty \sim 1$ cm/s, droplet diameters in the range of 0.5 m and $\alpha_1 \sim 10^{-4}$ cm^2/s, Pe $\sim$ 500 while Ja $\sim \theta(100)$ for droplets at the superheat limit. Translational effects are neglected (Equation 81). Also, $t_R/t_H \gg 1$ may not be satisfied so that the time-dependent term in the energy equation must be retained. As a result the energy (Equation 62) and momentum (Equation 59) equations must be solved simultaneously to describe the full evolution of the thermal boundary layer as it moves from the liquid 1/vapor interface out into liquid 1, and eventually penetrates into liquid 2.

The finite mass of vaporizing liquid is accounted for in two ways. First, the equation of motion (Equation 59) is integrated twice: first from R to S, and then from S to ∞. This yields two equations for the evolution of the pressure fields within the droplet and liquid 2. These equations are coupled by matching the radial velocities at the liquid 1/liquid 2 interface (viscous effects are neglected). Since there is no mass transfer across the liquid 1/liquid 2 boundary, the radial velocity is continuous across it. The velocity field within liquid 2 is then also described by Equation 58 (for the droplet geometry shown in Figure 16B). Combining Equations 58 and 59 integrating from R to S and again from S to ∞ yields

$$[\ddot{R}R + 2\dot{R}^2]\left(1 - \frac{R}{S}\right) - \varepsilon\frac{\dot{R}^2}{2}\left(1 - \frac{R^4}{S^4}\right) = \frac{1}{\rho_1\varepsilon}(P_{R1} - P_{S1}) \qquad R < r < S \tag{92}$$

$$[\ddot{R}R + 2\dot{R}^2]\frac{R}{S} - \varepsilon\frac{\dot{R}^2}{2}\frac{R^4}{S^4} = \frac{1}{\rho_2\varepsilon}(P_{S2} - P_o) \qquad S < r < \infty \tag{93}$$

Where P_{R1}, P_{S1}, and P_{S2} are defined in Figure 16B. These pressures are related to radius as

$$P - P_{R1} = \frac{2\sigma_1}{R} \tag{94}$$

$$P_{S1} - P_{S2} = \frac{2\sigma_{12}}{S} \tag{95}$$

where σ_{12} is the liquid 1/liquid 2 interfacial tension. Combining Equations 92–95 yields the equation of motion for a spherical bubble growing from the center of a spherical droplet:

$$[R\ddot{R} + 2\dot{R}^2]\left(1 - \bar{\varepsilon}\frac{R}{S}\right) - \varepsilon\frac{\dot{R}^2}{2}\left(1 - \bar{\varepsilon}\frac{R}{S}\right) = \frac{P - P_o}{\varepsilon\rho_1} - \frac{2\sigma_1}{\varepsilon\rho_1 R}\left(1 + \frac{\sigma_{12}}{\sigma_1}\frac{R}{S}\right) \tag{96}$$

where $\bar{\varepsilon} \equiv 1 - \rho_2/\rho_1$. When $S \to \infty$, or in the early stages of growth when $R \ll S$ and if the last term in Equation 96 is negligible, Equation 96 reduces to the classical Rayleigh equation (Equation 61). At later times when $R \to S$ the importance of dynamic effects resides in $\bar{\varepsilon}$; as $\bar{\varepsilon} \to 1$, dynamic effects will be unimportant when $R \to S$. In general, the time domain over which Equation 96 has to be included in the analysis may be small—less than the first few milliseconds after nucleation.

Secondly, the temperature field is a two-domain problem. The energy equations for liquids 1 and 2 (Equation 62 with i = 1, 2) are coupled by interface matching conditions. These equations are the following:

$$\frac{\partial T_1}{\partial t} = \frac{\alpha_1}{r^2}\frac{\partial}{\partial r}\left(r^2\frac{\partial T_1}{\partial r}\right) - \varepsilon\frac{\dot{R}R^2}{r^2}\frac{\partial T_1}{\partial r} \qquad R < r < S \tag{97}$$

and

$$\frac{\partial T_2}{\partial t} = \frac{\alpha_2}{r^2}\frac{\partial}{\partial r}\left(r^2\frac{\partial T_2}{\partial r}\right) - \varepsilon\frac{\dot{R}R^2}{r^2}\frac{\partial T_2}{\partial r} \qquad S < r < \infty \tag{98}$$

The interface boundary conditions are the following:

$$T_1(r, 0) = T_2(r, 0) = T_o \tag{99a}$$

$$T_1(R, t) = T_v \tag{99b}$$

$$T_1(S, t) = T_2(S, t) \tag{99c}$$

$$k_1\frac{\partial T_1}{\partial r}(S, t) = k_2\frac{\partial T_2}{\partial r}(S, t) \tag{99d}$$

$$T_2(\infty, t) = T_o \tag{99e}$$

where T_o is the kinetic limit of superheat corresponding to the applied pressure P_o. An energy balance applied to the vapor/liquid 1 interface with spherical symmetry yields again Equation 63b. This equation relates the bubble growth rate to the temperature field, while the momentum equation, Equation 96, relates P to t.

The statement of the problem is made more general by introducing the following nondimensional quantities:

$$\bar{T} = \frac{T - T_s}{T_o - T_s} \qquad \bar{r} = \frac{r}{S_o} \qquad \bar{R} = \frac{R}{S_o}$$

$$\dot{\bar{R}} = \frac{RS_o}{\alpha_1} \qquad \tau = \frac{t\alpha_1}{S_o^2} \qquad \gamma = \frac{\alpha_2}{\alpha_1}$$

$$\zeta = \frac{k_2}{k_1} \qquad Ja = \frac{\rho_1 C_{\rho 1}(T_o - T_s)}{\rho_v h_{fg}} \qquad \bar{\sigma}_{12} = \frac{2\sigma_{12}S_o}{\alpha_1^2 \rho_1 \varepsilon}$$

$$a_p = \frac{S_o^2}{\alpha_1 \rho_1 \varepsilon}\{P(T_o) - P_o\} \qquad \bar{P} = \frac{P(T_v) - P_o}{P(T_o) - P_o} \qquad \bar{\sigma}_1 = \frac{2\sigma_1 S_o}{\alpha_1^2 \rho \varepsilon}$$

Equations 96–98 then become

$$[\ddot{\bar{R}}\bar{R} + 2\dot{\bar{R}}^2]\left(1 - \bar{\varepsilon}\frac{\bar{R}}{\bar{S}}\right) - \frac{\varepsilon\dot{\bar{R}}^2}{2}\left(1 - \bar{\varepsilon}\frac{\bar{R}^4}{\bar{S}^4}\right) = a_p\bar{P} - \frac{\bar{\sigma}_1}{\bar{R}}\left[1 + \frac{\bar{\sigma}_{12}}{\bar{\sigma}_1}\frac{\bar{R}}{\bar{S}}\right], \qquad R < r < \infty \tag{100}$$

$$\frac{\partial \bar{T}_1}{\partial \tau} = \frac{1}{\bar{r}^2}\frac{\partial}{\partial \bar{r}}\left(\bar{r}^2\frac{\partial \bar{T}_1}{\partial \bar{r}}\right) - \frac{\varepsilon\dot{\bar{R}}\bar{R}^2}{\bar{r}^2}\frac{\partial \bar{T}_1}{\partial \bar{r}}, \qquad \bar{R} < \bar{r} < \bar{S} \tag{101}$$

and

$$\frac{\partial \bar{T}_2}{\partial \tau} = \frac{1}{\bar{r}^2}\frac{\partial}{\partial \bar{r}}\left(\bar{r}^2\frac{\partial \bar{T}_2}{\partial \bar{r}}\right) - \frac{\varepsilon\dot{\bar{R}}\bar{R}^2}{\bar{r}^2}\frac{\partial \bar{T}_2}{\partial \bar{r}} \qquad \bar{S} \le \bar{r} < \infty \tag{102}$$

subject to the following initial and boundary conditions

$$\bar{T}_1(\bar{r}, 0) = \bar{T}_2(\bar{r}, 0) = 1 \tag{103a}$$

$$\bar{T}_1(\bar{R}, \tau) = \bar{T}_v \tag{103b}$$

$$\bar{T}_1(\bar{S}, \tau) = \bar{T}_2(\bar{S}, \tau) \tag{103c}$$

$$\frac{\partial \bar{T}_1}{\partial \bar{r}}(\bar{S}, \tau) = \zeta\frac{\partial \bar{T}_2}{\partial \bar{r}}(\bar{S}, \tau) \tag{103d}$$

$$\bar{T}_2(\infty, \tau) = 1 \tag{103e}$$

Equation 63b is nondimensionalized to:

$$Ja\left.\frac{\partial \bar{T}}{\partial \bar{r}}\right|_{\bar{r}=\bar{R}} = \dot{\bar{R}} \tag{104}$$

No known analytical solution to Equations 100–104 exists so numerical methods must be employed. The main difficulty with a numerical solution is the existence of two moving boundaries: at the liquid 1/vapor interface, and at the liquid 1/liquid 2 interface. A coordinate system which immobilizes these boundaries facilitates a solution. Such a coordinate transformation was first utilized by Duda et al. [106] in connection with analyzing growth of a single vapor bubble in an unbounded atmosphere (in which there is only one moving boundary), and later generalized by Saitoh [107] to boundaries of arbitrary shape. This transformation is illustrated in Figure 19 and

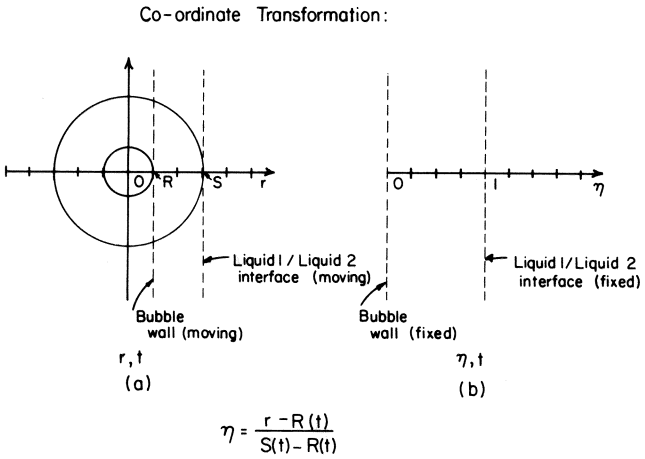

Figure 19. Coordinate transformation to immobilize moving boundaries in a bubble/droplet system.

expressed as

$$\eta = \frac{\bar{r} - \bar{R}}{\bar{S} - \bar{R}} \tag{105}$$

Time is untransformed. Introducing this transformation into Equations 101 and 102 yields

$$A_i(\eta, \tau)\frac{\partial \bar{T}_i}{\partial \tau} = \frac{\partial}{\partial \eta}\left[B_i(\eta, \tau)\frac{\partial \bar{T}_i}{\partial \eta}\right] - D_i(\eta, \tau)\frac{\partial \bar{T}_i}{\partial_\eta} \tag{106}$$

with

$$A_i(\eta, \tau) = \bar{r}^2(\bar{S} - \bar{R})/d_i$$

$$B_i(\eta, \tau) = \bar{r}^2/(\bar{S} - \bar{R})$$

$$D_i(\eta, \tau) = \left[\varepsilon\bar{R}^2 + \frac{\bar{r}^3(\bar{S}^2 - \varepsilon\bar{R}^2) - \bar{r}^2}{\bar{S}^2(\bar{S} - \bar{R})^2}\right]\dot{\bar{R}}/d_i \tag{107}$$

where $i = 1, 2$

$$d_1 = 1 \qquad (0 \le \eta < 1) \tag{108a}$$

$$d_2 = \gamma \qquad (0 \le \eta < \infty) \tag{108b}$$

and

$$\bar{r} = \eta(\bar{S} - \bar{R}) + \bar{R} \tag{108c}$$

The transformed initial and boundary conditions are:

$$\bar{T}_1(\eta, 0) = \bar{T}_2(\eta, 0) = 1 \tag{109a}$$

$$\bar{T}_1(0, \tau) = 0 \tag{109b}$$

$$\bar{T}_1(1, \tau) = \bar{T}_2(1, \tau) \tag{109c}$$

$$\left.\frac{\partial \bar{T}_1}{\partial \eta}\right|_{\eta=1} = \zeta \left.\frac{\partial \bar{T}_2}{\partial \eta}\right|_{\eta=1} \tag{109d}$$

$$\bar{T}_2(\infty, \tau) = 1 \tag{109e}$$

Finally, the interface heat balance is transformed to

$$\dot{\bar{R}} = \frac{\mathrm{Ja}}{(\bar{S} - \bar{R})} \left.\frac{\partial \bar{T}_1}{\partial \eta}\right|_{\eta=0} \tag{110}$$

The momentum equation (Equation 100) is independent of r and unaffected by this variable transformation.

The transformation of Equation 105 makes the transformed energy equation much more complicated. This is more than compensated by the ability to apply the boundary conditions simply and accurately in the numerical scheme. No assumptions regarding the thickness of the thermal boundary layer or neglect of thermal resistance of liquid 1 have been made in Equation 106–110.

A Crank-Nicholson method was used to solve Equations 100 and 106–110 simultaneously at each time step [108]. The initial bubble size was perturbed by 10^{-4} to 10^{-5} to start the computations. The radius of the droplet, $\bar{S}$, is related to the bubble radius, $\bar{R}$, at any time by

$$\bar{S} = (1 + \varepsilon \bar{R}^3)^{1/3} \tag{111}$$

Computations were terminated when liquid 1 was completely vaporized (Equation 1). The final bubble is not in thermal equilibrium with liquid 2 and restoration of equilibrium requires a further expansion of the bubble beyond $\bar{R}_f$ attendant to its temperature increasing from T_v to T_o. This expansion is very small and was neglected.

Four nondimensional groups control the radius-time history of the bubble: Ja, $\bar{\varepsilon}$, γ, and ζ. Calculations were performed for values of these parameters typical of hydrocarbon (liquid 1)/glycerine (liquid 2) and hydrocarbon/water combinations.

The solution may be broadly divided into two regions:

1. A period during which the thermal boundary layer resides in liquid 1 and growth is similar to growth in an infinite medium.
2. A later stage of growth characterized by thermal boundary-layer penetration into liquid 2.

Early stages of growth. Several aspects of bubble growth in the early stages wherein the thermal boundary layer resides entirely in the droplet are identical to bubble growth in an infinite medium. This is illustrated in Figure 20 which shows the evolution of P, T_v, and $\bar{R}$ for a bubble growing in an n-octane droplet in glycerine (liquid 2) at Ja = 10. The initial state of the droplet (T_o and $P(T_o)$) corresponds to the limit of superheat as calculated by methods described earlier. The asymptotic temperatures and pressures ($T_v(P_o)$ and $P(T_s)$) correspond to saturation conditions. The results shown in Figure 20 are identical to what would be obtained if the n-octane droplet were considered to be of infinite radius and $\bar{\varepsilon} \sim 1$.

Figure 21 illustrates the variation of bubble radius during this very early period. The initial radius ($\bar{R}_o$ in Figure 21) corresponds to the unstable state of the critical nucleus. The characteristic

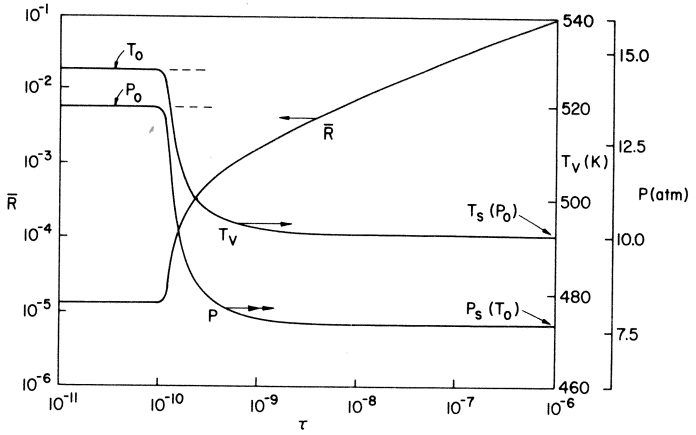

Figure 20. Early time variation of vapor pressure, and vapor temperature, and radius of a bubble growing in a superheated n-octane droplet using model shown in Figure 16B. Initial conditions correspond to kinetic limit of superheat of octane at indicated pressure.

delay period is shown, followed by relaxation of surface tension and attendant rapid increase in growth rate. These characteristics are similar to those for growth in an infinite medium (e.g., [76]).

The temperature field within the droplet during this early period is shown in Figure 22 for the special case Ja = 10. The evolution of both the thermal boundary layer ($\bar{\delta}$ where $\bar{T} \to 1$) and vapor temperature $\bar{T}$ ($\eta = 0$) are indicated. For $\tau > 5 \times 10^{-8}$, $\bar{T}$ ($\eta = 0$) $\to 0$ and the analysis becomes a purely thermal problem; the thermal boundary layer is still close to the bubble wall ($\bar{\delta} \sim 10^{-4}(\bar{S} - \bar{R})$). The bubble itself, though, is still quite small at this time (Figure 22).

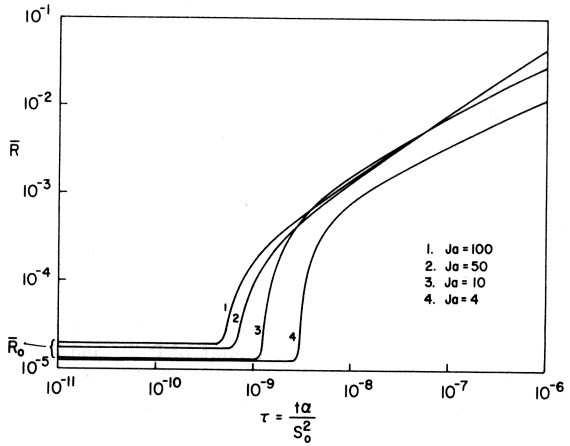

Figure 21. Variation of bubble radius with time at various Jakob numbers (ie., superheats) during early stages of bubble growth in an n-octane droplet.

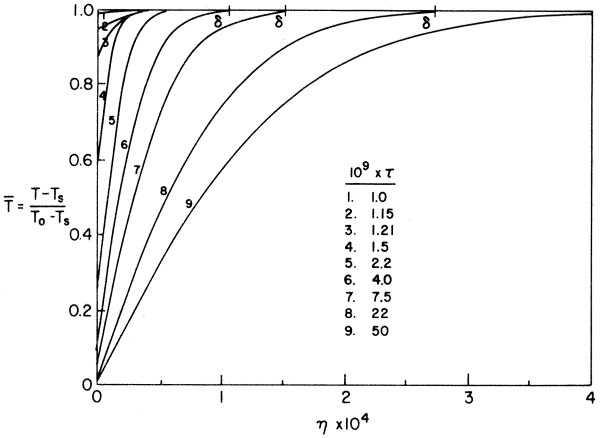

Figure 22. Variation of liquid temperature with position in a droplet at various early times such that thermal boundary layer (δ) is still within the droplet and vapor temperature is changing with time ($\bar{T} > 0$ at $\eta = 0$) [108]. Ja = 10, $\varepsilon = 0.995$, $\zeta = 5$, and $\gamma = 1$.

Later stages of growth. Eventually the thermal boundary layer will extend into liquid 2 before liquid 1 completely evaporates and the energy equation for liquid 2, and associated matching conditions at the interface (Equation 109) must be included in the analysis. Figure 23 illustrates calculated temperature fields at various times for Ja = 10, $\varepsilon = 0.995$ (a hypothetical value), $\zeta = 5$, and $\gamma = 1$. For $\tau > 0.006$ the thermal boundary layer extends into liquid 2. The essentially linear temperature profile in liquid 1 for $\tau > 0.01$ shown in Figure 23 could lead to simplifications in the

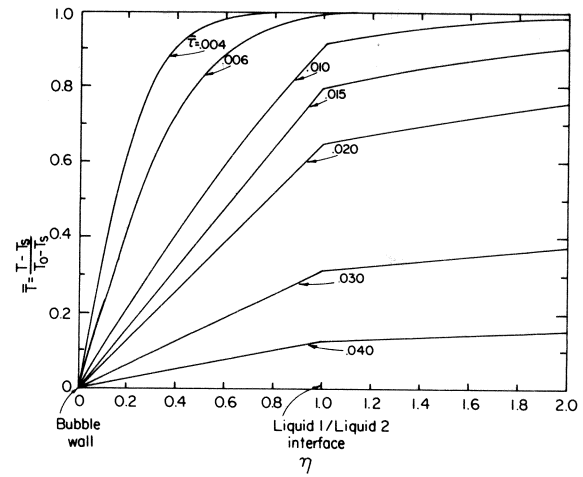

Figure 23. Variation of liquid temperature with position in a droplet showing evolution of temperature field $T \to 0$ at $\eta = 0$. For $\tau \gtrsim 0.006$ boundary layer enters liquid 2. Ja = 10, $\varepsilon = 0.995$, $\zeta = 5$, and $\gamma = 1$.

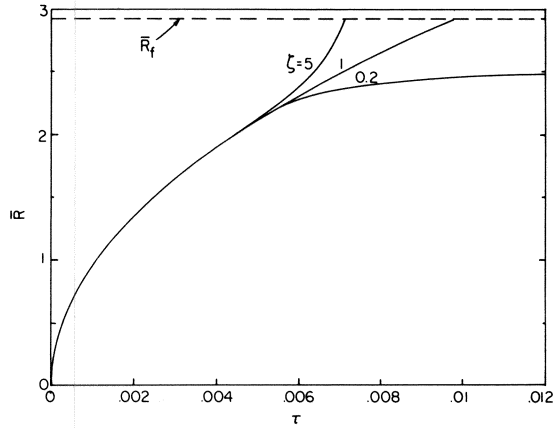

Figure 24. Evolution of bubble radius ($\bar{R}$) with time (τ) showing effect of ζ for $\gamma = 1$, Ja = 10, and $\varepsilon = 0.96$. (Properties of n-octane at its superheat limit.)

analysis which have not been fully explored. The corresponding simplification associated with condensation of vapor on an immiscible liquid droplet has been previously studied [109].

The effect of thermal boundary-layer penetration in liquid 2 on bubble growth rate is shown in Figures 24 and 25 for the indicated ranges of Ja, γ, and ζ. Growth is independent of liquid 2 properties up to some time, after which the bubble (and droplet) growth rate undergo rather dramatic changes, depending on the values of ζ and γ. This initial period where liquid 2 does not effect growth reflects the fact that the thermal boundary layer is still within liquid 1. $\zeta > 1$ implies a less steep temperature gradient in liquid 2 than in liquid 1. This in turn creates a gradient in liquid 1 at $\eta = 1$ larger than would be realized if $\zeta = 1$ (i.e., when properties of liquids 1 and 2 are identical). This increased temperature gradient at $\eta = 1$ translates into a larger temperature gradient at $\eta = 0$ (the bubble wall). The bubble then experiences an increase in its growth rate. This behavior cannot be predicted from an analysis which (1) neglects the thermal resistance of liquid 1, and/or (2) assumes results from growth in an infinite medium apply to this problem.

Similar effects occur when γ varies while ζ is fixed. This is illustrated in Figure 26 for Ja = 10. The bubble grows faster as γ decreases. For example, a lowering of γ means that the heat capacity per unit volume of liquid 2, $\rho_2 Cp_2$, is increased. The ability of liquid 2 to supply more heat to

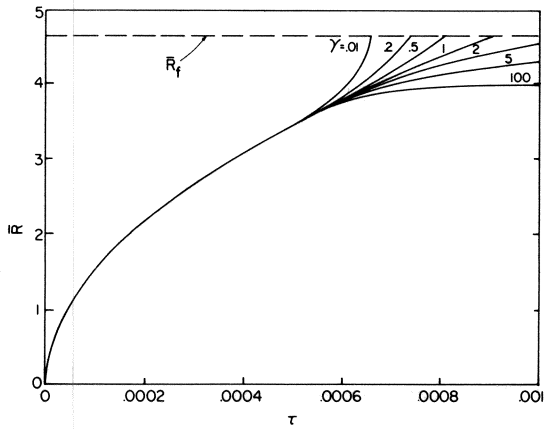

Figure 25. Evolution of bubble radius showing effect of γ for $\zeta = 1$, Ja = 10, and $\varepsilon = .96$.

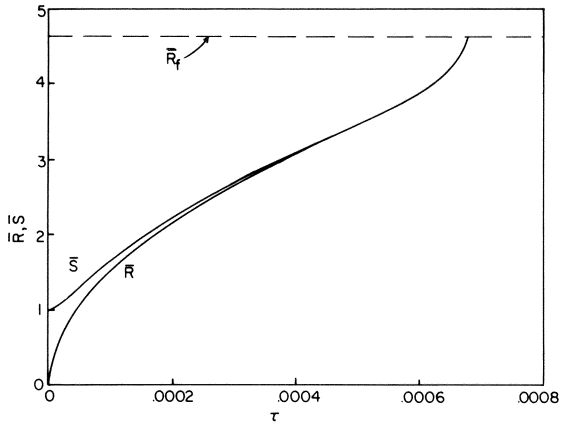

Figure 26. Evolution to both bubble ($\bar{R}$) and droplet ($\bar{S}$), radii for Ja = 50 and $\zeta = 5.0$. Curves terminate when $\bar{R} \rightarrow \bar{S} = \bar{R}_f$ and the droplet is completed evaporated.

liquid 1 is then increased as γ decreases, and the growth rate correspondingly increases when the thermal boundary layer enters liquid 2.

The very early period of growth wherein the momentum equation is needed to describe the evolution of pressure field is undetectable on the scale of Figures 24 and 25 (cf., Figure 22). For the time scales in these figures $P \simeq P_o$ and $\bar{T}(\eta = 0) \simeq 0$, though there will always (at least numerically) be a nonzero difference in pressure across the evaporating boundary. The effect of this small pressure difference on growth rate is negligible for conditions of the calculations appearing in Figures 24 and 25.

As liquid 1 evaporates, both the internal vapor bubble and the droplet as a whole expand. Figure 26 illustrates a typical evolution of $\bar{S}$ and $\bar{R}$ for Ja = 50 for one representative set of conditions. When $\bar{R} \rightarrow \bar{S}$, the droplet is completely vaporized. It is worth noting that the droplet is almost completely taken up by vapor with just a thin layer of liquid 1 around it when $\tau \geq 2 \times 10^{-4}$.

As the Jakob number increases, the time for which liquid 2 effects growth (i.e., when $\bar{\delta} > \bar{S} - \bar{R}$) increases and the characteristic "fanning" of the growth curves shown in Figures 24 and 25 originates at progressively larger times. For sufficiently high Jakob number the thermal boundary layer remains within liquid 1 throughout nearly the entire period of evaporation, except when $\bar{S} \rightarrow \bar{R}$ at which time the boundary layer must contact the droplet boundary. Growth is then independent of liquid 2 properties. Figure 27 illustrates this for Ja = 100. At this high Jakob number, $\bar{T}(\eta = 0) \rightarrow 0$ at times much shorter than indicated in Figure 27.

For purely heat-transfer-controlled growth, a simplified analysis similar to that formulated by Sideman and Isenberg [22] (in which they used the quasi-steady approximation) has recently been presented [11] based on the droplet geometry shown in Figure 28. Thermal boundary layers were assumed to be close to the bubble (Ja $\gg$ 1) over the time domain characteristic of the experiments reported in Reference 11 (< 100 ms). These boundary layers were approximated as growing according to the classic planar variation of

$$\delta_i \sim (c_i \alpha_i t)^{1/2}$$

A simple energy balance around the two-phase droplet yields

$$\frac{d\bar{S}}{d\tau} = \frac{Ja\varepsilon}{4c_1}(2 - Z)\left[Z + \zeta\left(\frac{c_1}{c_2} \cdot \frac{1}{\gamma}\right)^{1/2}\right]\tau^{-1/2} \tag{112}$$

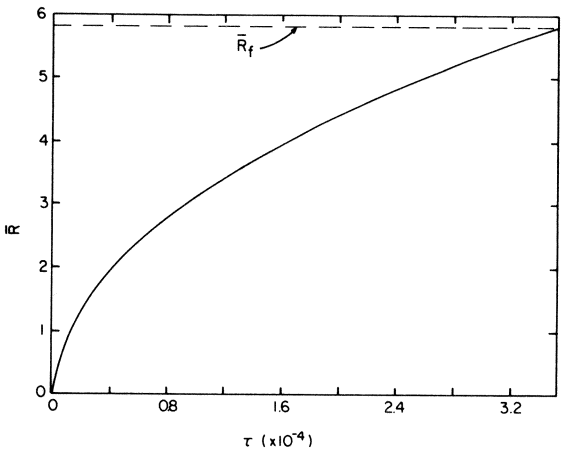

Figure 27. Evolution of bubble radius within a droplet when thermal boundary layer resides within droplet throughout its entire evaporation. Ja = 100 and $\varepsilon = 0.995$.

where Z (a geometrical factor) is given by

$$Z = 2\cos\left[\frac{1}{3}\cos^{-1}\left\{1 - \frac{1-(1-\varepsilon)\bar{S}^3}{\varepsilon\bar{S}^3}\right\} + \frac{4\pi}{3}\right] + 1 \tag{113}$$

The constants c_1 and c_2 were essentially considered as empirical values. Equations 111 and 112 provide an alternative to Equations 66 or 87 for correlating bubble growth data in liquid droplets by judiciously selecting c_1 and c_2 when growth is heat-transfer-controlled. However, numerical integration will be required which may make such efforts cumbersome.

It is interesting to explore the similarity of heat-transfer-controlled bubble growth in a droplet to the bubble growth law characteristic of an infinite medium (Equation 66 with $q = \frac{1}{2}$. For this purpose calculations for Ja = 10, $\zeta = 1$, and $\varepsilon = 0.9995$ (a hypothetical value chosen so that $\bar{S} \to \bar{R}_f$ at a time large enough to clearly illustrate the similarity) are displayed in Figure 29 on a logarithmic scale for three values of γ. When $\gamma = 1$ the indicated line is identical to the asymptotic heat transfer limit of Equations 66 and 67–70 [77] regardless of placement of the thermal boundary layer. For general γ and $\tau \lesssim 1.1 \times 10^{-2}$ in Figure 29 the thermal boundary layer extends into liquid 2. q may

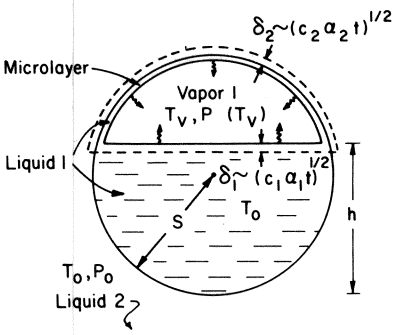

Figure 28. Model for heat-transfer-controlled growth when thermal boundary layer remains close to the evaporating boundary [11].

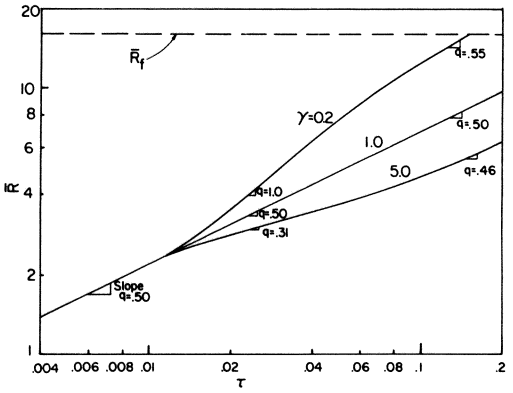

Figure 29. Effect of time (τ) on bubble growth exponent (Equation 66) for heat transfer controlled growth of a bubble in a droplet at various γ and $\zeta = 1$, Ja = 10, and $\varepsilon = 0.9995$ (a hypothetical value). Thermal boundary layer penetrates into liquid 2 at $\tau \lesssim .011$.

then be larger or smaller than $\frac{1}{2}$. When $\gamma > 1$, the temperature gradient in liquid 2 is larger than the corresponding gradient in liquid 1. The growth rate decreases compared to the infinite medium case and $q < \frac{1}{2}$. The opposite is true when $\gamma < 1$. Eventually as $\bar{\delta} \gg \bar{S} - \bar{R}$, the thermal resistance of liquid 1 becomes of negligible importance, and the temperature field resembles that which would exist for a bubble growing in an infinite medium of liquid 2 (through ρ_v and h_{fg} would be that corresponding to liquid 1); again $q \to \frac{1}{2}$. In general q will be a function of the depth of penetration of the thermal boundary layer into liquid 2. This fact could be useful in correlating experimental bubble growth data in a liquid droplet, using Equation 66, similar to its utility in correlating bubble growth in an infinite medium (eg., [110]).

Exploding Droplets

The present discussion has not specifically addressed the origin of vapor explosions of droplets commonly observed in the experimental methods discussed in the next section. Such explosions are defined by the appearance of shock blast waves of such a magnitude as to create an audible sound when the droplet vaporizes. The origin of these waves is evidently the very rapid movement and high mass flux at the bubble wall. The theory outlined in the preceding discussion requires modification in light of some recent experiments.

A mechanism to explain explosive growth of bubbles in liquid droplets has been offered by Shepherd and Sturtevant [18] which is a significant departure from the classical approach previously discussed. Under certain conditions (low ambient pressures and high superheats for many organic liquids), the bubble surface is not smooth (such as occurs at high pressures [11]), but rather rough and appears wrinkled thus giving the appearance of waves. The mass evaporative flux across such wrinkled evaporating boundaries was estimated to be two orders of magnitude greater than that calculated from knowledge of just the bubble radius history, ρ_v dR/dt where ρ_v is effective vapor density inside the bubble and R is bubble radius.

Figure 30 shows that measured bubble growth data [18] obtained under explosive conditions are actually bounded by the classical theory—corresponding to bubble growth in an infinite media (relevant in view of the very early times at which the indicated data were obtained—the first few *micro* seconds after nucleation). This similarity between predicted and observed bubble radii is probably fortuitous. The presence of comparatively large observed evaporative mass fluxes during explosive vaporization of droplets at the superheat limit (i.e., a vaporization generating blast waves in the surrounding liquid) led Shepherd and Sturtevant to conjecture the existence of an instability at the interface driven by mass transfer which effectively wrinkles and distorts it. Similar to the inertial instability first introduced by Landau [111] in connection with the instability of laminar flames, this kind of instability may now also be present in the vapor explosion of liquid droplets at their superheat limit [18]. At elevated pressures, or for certain miscible mixtures which contain

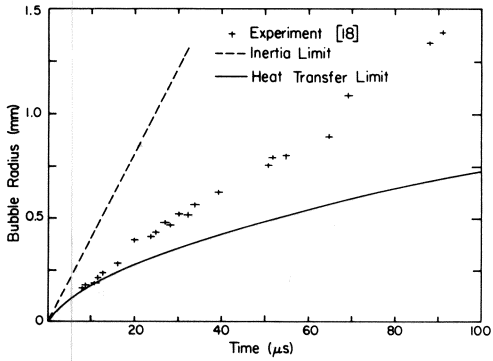

Figure 30. Variation of bubble radius with time during the first few microseconds after homogeneous nucleation in an n-butane droplet at 0.101MPa. Calculations correspond to purely thermally or dynamically driven growth [18].

a nonvolatile component, the interfacial instability at the bubble surface is not present [11, 15], and vaporization is not explosive. Further work is needed to explore in greater depth this interesting new idea.

EXPERIMENTAL METHODS

The principle experimental method used to study superheated liquid droplets involves encapsulating a droplet of the volatile liquid (liquid 1) in another immiscible field liquid (liquid 2), and then subjecting the field liquid to such conditions as to bring the encapsulated droplet into the metastable state. These conditions have consisted of isobarically heating the field liquid [11, 15, 16, 18, 28, 29, 41, 48, 65, 74, 97, 112–122] or isothermally decompressing it [30, 95, 123, 124]. The corresponding loci of states the test droplet experiences as it approaches its limit of superheat are illustrated by paths a-c and b-c in Figure 2A. When the droplet vaporizes, the ambient pressure and temperature are inferred from corresponding measurements in liquid 2 (due account being taken of any droplet underheating). This method, coupled with high speed cine [11, 27, 28, 125] or spark gap [18] photography, has yielded essentially all the information which forms the foundation of our understanding of bubble growth within liquid droplets at the superheat limit. The first demonstration of the existence of superheated liquids was made over 100 years ago by a variant of this "floating droplet" method [126, 127].

The chief advantage of heating droplets suspended in immiscible liquids resides in the fact that the liquid 1/liquid 2 interface constitutes a hypothetically ideal smooth surface free of any solid motes or trapped gases which would tend to initiate a phase transition. This interface has essentially a similar microscopic structure as the bulk of the droplet. Any phase transition at this interface would therefore have to occur by essentially the same mechanism as in the bulk of the test droplet.

The key to successful use of this method is to carefully select the liquid 1/liquid 2 combination to satisfy the following criteria:

1. The field liquid must have a boiling point higher than the limit of superheat of the most nonvolatile component within the liquid 1 droplet over the entire range of ambient pressures at which the limit of superheat is to be measured.
2. Both liquids must have low mutual solubility.
3. The physical properties of both liquids should be available (or predictable).
4. The probability for nucleation within the bulk of the test droplet must be higher than at the droplet/field liquid interface.

As we have seen from Equation 74c, this latter requirement dictates that liquid 2 has a relatively high surface tension. Otherwise, measured phase transition states will essentially have character-

ized the interface between the two liquids rather than the test liquid itself. Such temperatures (at a given pressure) are generally far below those indicative of homogeneous nucleation in the bulk of the test droplet. This fact limits the extent of the various liquids which can be tested by floating droplet methods. Nevertheless, the method, when the preceding criteria are satisfied, has yielded some of the most reproducible and accurate superheat limit (and all bubble growth) data thus far reported.

Two principal variants of the suspended droplet method have been used. The first involves droplets moving through a static field liquid, and the second involves levitating the droplets in either a moving field liquid or via imposing a standing acoustic wave on a static field liquid (e.g., see Reference 64).

In the first method, the field liquid is usually heavier than the droplet, though experiments with heavy droplets heated in light field liquids have also been performed [17, 95]. A schematic diagram of a typical apparatus of this genre is shown in Figure 31. The first to use a variant of this apparatus were Wakeshima and Takata [121] and Moore [95]. The essential components consist of a vertical tube (called a "bubble column") which contains the field liquid on which a stable temperature gradient is imposed (e.g., hot at the top of the tube and cold at the bottom for light droplets), a droplet injector, and instrumentation to measure the temperature and pressure in the field liquid at which the droplets vaporize. The bubble column itself is glass with inside diameters which have ranged from as small as 1.3 cm [74] to over 6 cm [18]. Tube length has ranged from 100 cm [112] down to 35 cm [121, 122]. Temperature gradients imposed on the field liquid have been effected by heating nichrome wire wrapped around the tube with varying pitch, a metal sleeve fitted around the tube with attached electrical heater, or commercially available rope heaters. Temperature gradients have ranged from 0.03 K/cm [48] to 10 K/cm [119]. For typical rise velocities of 1 cm/s to 5 cm/s, test droplets are heated at rates ranging from 0.03 K/s to 50 K/s.

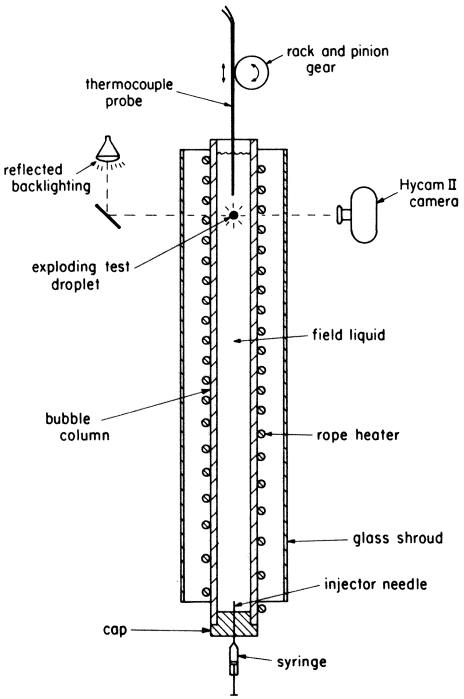

Figure 31. Schematic illustration of a typical bubble column apparatus for superheating liquid droplets by isobaric heating.

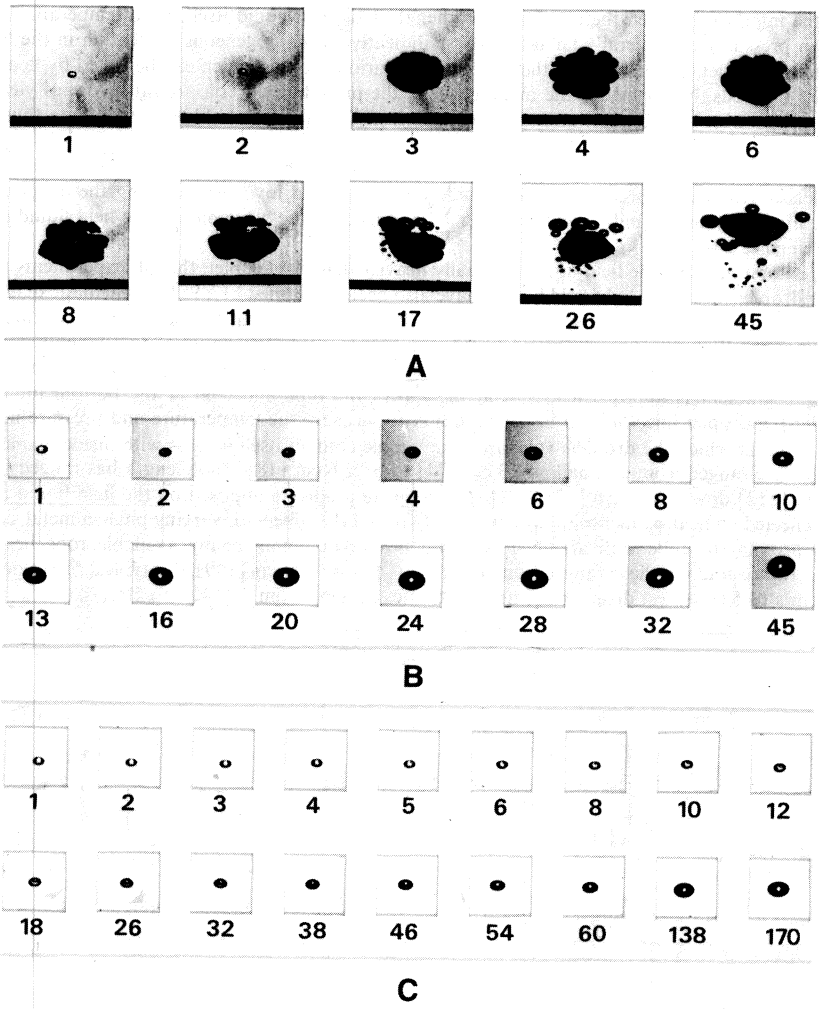

Figure 32. High speed motion picture sequence of n-octane droplets boiling in glycerine. Number of frame in the motion picture sequence is shown below each photograph [11]:
(A) $P_0 = 0.101$ MPa, $T_0 \simeq 514$ K, $S_0 \simeq 0.05$ mm, framing rate = 1,033 frames/s;
(B) $T_0 = 0.687$ MPa, $T_n \simeq 525$ K, $S_0 \simeq 0.6$ mm and framing rate = 933 frames/s;
(C) $P_0 = 1.22$ MPa, $T_0 \simeq 531$ K, $S_0 = 0.5$ mm and framing rate = 900 frames/s.

The use of high-speed cine photography with this method to measure droplet expansion rates [11, 27, 28] requires proper synchronization between the emergence of the moving droplet in the field of view of the (stationary) camera and activation of the camera. This fact limits the usefulness of this photographic technique for recording the dynamics of vaporization, inasmuch as some luck is involved with synchronizing the activation of the camera with the start of boiling. The maximum camera framing rate is limited to that which will yield a high probability of recording vaporization.

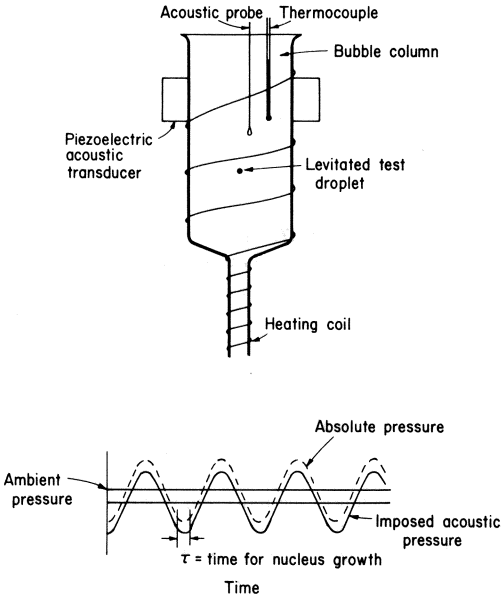

Figure 36. Schematic illustration of apparatus (A) which levitates superheated droplets by exposure to a standing acoustic wave. Thypical wave form shown in (B) [30].

flow rate, a light test droplet injected at the bottom of the test chamber could be levitated. The experiment as illustrated was designed to study the effect of a dissolved gas (nitrogen) on the superheat limit of a single component fluid (ether) over a range of pressures. Droplet vaporization was not photographically documented. The droplet levitation method employed by Apfel [28, 30] (Figure 36) consisted of imposing a standing acoustic wave on liquid 2 (by a piezoelectric transducer cemented to the walls of the bubble column) of such a magnitude that the force of the acoustic pressure just balanced the buoyancy force of the droplet. With the droplet levitated, it was stressed for those periods of exposure to the negative parts of the acoustic cycle (Figure 36B). When the magnitude of the negative pressure is high enough and of long enough duration, any cavities formed by homogeneous nucleation will grow to observable size; otherwise the bubble will collapse as the acoustic pressure becomes positive. Measured tensile strengths were found to be in excellent agreement with predicted values for several organic liquids. This was the first such agreement using any experimental method for measuring tensile strengths of liquids. Apfel and Harbison [28] later used high-speed (3,500 frames/s) cine photography to measure expansion rates of ether droplets at atmospheric pressure. The same problem of synchronizing camera activation with initiation of vaporization apparently existed with this levitation method as with the rising droplet method.

Basic information obtained from the previously mentioned experiments consisted of temperature and pressure of liquid 2 at which droplets were observed to vaporize; when photographic methods were employed to record vaporization of the test droplets, droplet radius as a function of time was also measured (the methods employed were sufficiently imprecise to resolve the evolution of internal bubble radii (R) so that only overall droplet radii (S) could accurately be measured).

Figures 32–34 illustrate a series of photographs of n-octane, n-butanol, and ether droplets, respectively, boiling in various field liquids. The droplets are at their (approximate) superheat limits at pressures ranging from atmospheric to about 12 atm. It is evident that vaporization at atmospheric pressure occurred at a time between the first two frames of the motion picture sequences shown in Figures 32A–34, and thus in less than 1 ms. For the vaporization shown in these pictures the droplets vaporized with an audible sound and resembled a kind of mini explosion. Subsequent events illustrate droplets which have completely vaporized inasmuch as the bubble shown in the second or third frame in Figures 32A–34 either corresponds to that predicted by Equation

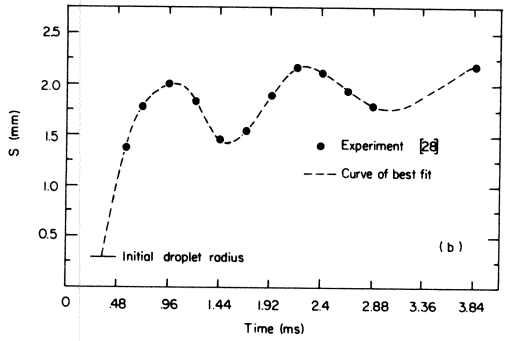

Figure 37. Measured temporal variation of radius of an ether droplet vaporizing in glycerine at its superheat limit. $P_0 \simeq -0.8$ MPa and $T \simeq 413$ K [28].

1 or is larger. For this kind of explosive vaporization, the final bubbles were always observed to oscillate. Such oscillations are believed to be a result of the kinetic energy stored in the outward motion of the vapor/liquid interface moving the interface beyond its final equilibrium size, and then contracting as the ambient liquid pressure counterbalances the reduction in gas pressure due to this expansion [18, 28]. Some measurements of droplet radii during oscillatory motion of an ether bubble during this oscillatory motion are shown in Figure 37 [28]. A theory to explain and predict the origin of these oscillations has not yet been developed. The line shown in Figure 37 is a best fit through the data; the analysis of the previous section does not account for bubble oscillations.

A unique improvement of the method of photographically recording rapid (explosive) evaporation of droplets at the superheat limit has recently been developed by Shepherd and Sturtevant [18]. This method resolves the early time domain (< 1 ms) which is inaccessible using conventional high speed cine photography. The technique consists of using the pressure signal generated on a piezoelectric pressure transducer (immersed in liquid 2) by the blast wave created by an exploding droplet to trigger a spark gap light source with a variable time delay. Effective observation times are thus on the order of *microseconds*. The evolution of phase change of a single droplet is pieced together from individual observations of a number of droplets, each of which is photographed at progressively later times in the vaporization process. Fortunately, the vaporization process is sufficiently repeatable that this does not create problems.

Figure 38 illustrates several photographs of n-butane droplets vaporizing in glycerine at atmospheric pressure which were taken using this technique. Times range from 9 μs to about 70 μs after homogeneous nucleation. It is clear that the detail depicted in these photographs is completely missed using photographic methods which operate on a millisecond time scale. This detail also permits direct measurement of bubble radius (R) in addition to overall droplet radius (S). The results are suggestive of only one bubble having been nucleated within the initial butane droplet (1 mm diameter). This bubble apparently nucleates at a more or less random location at the droplet boundary (where the temperature is highest due to droplet underheating). As is shown in Figure 38, the evaporating boundary is apparently wrinkled and wave-like. This nonsmooth surface persists well into the oscillatory phase after complete evaporation (cf., Figure 33). The origin of this wrinkling requires further investigation. Several other salient features of explosive vaporization of droplets are discussed in Reference 18.

At sufficiently high pressures, droplets at the superheat limit do not vapor explode inasmuch as

- No audible sound is generated on vaporization.
- No oscillations occur.
- The evaporating boundary is smooth.

Figures 32B and 32C clearly illustrate this for n-octane droplets in glycerine at 0.687 MPa and 1.22 MPa [11] (the indicated temperature is the n-octane superheat limit). As noted in these figures,

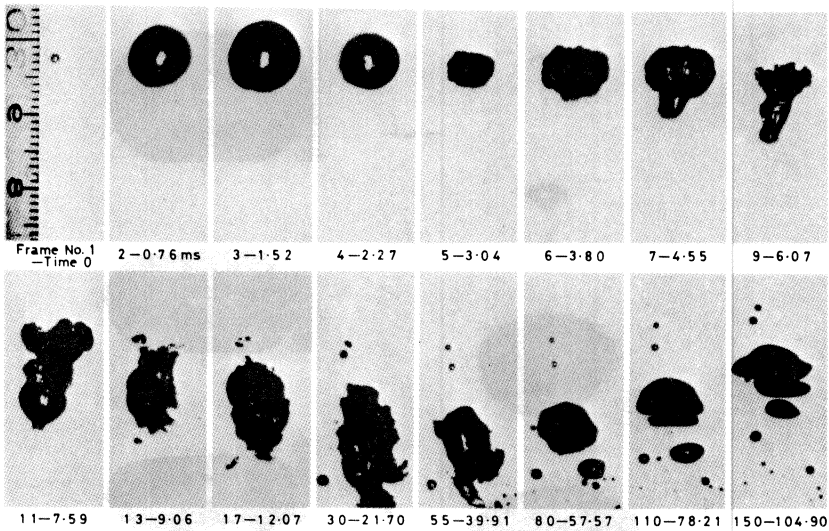

Figure 34. Motion picture sequence of an ether droplet boiling in glycerine. Number below each photograph indicates time elapsed after frame no. 1. $P_0 = 0.101$ MPa, $T = 421$ K, and $S_0 = 0.55$ mm [125].

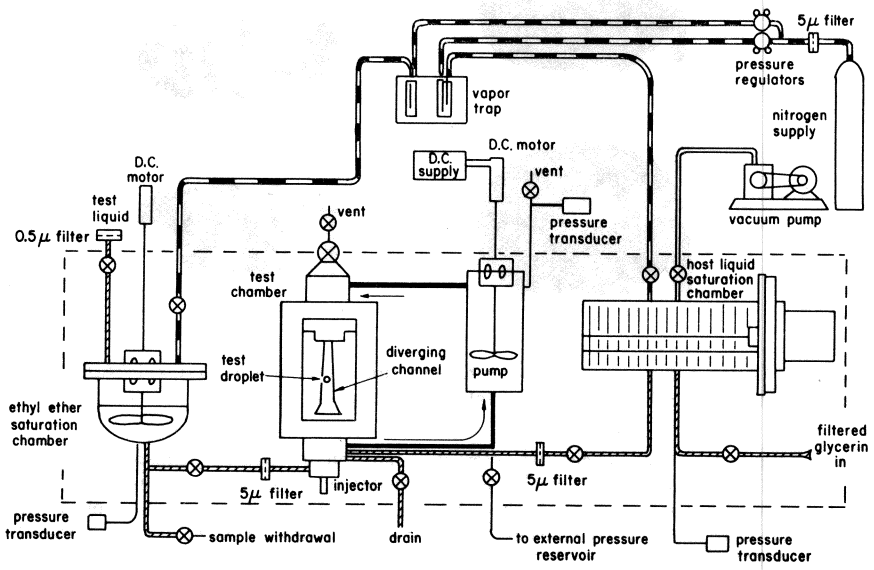

Figure 35. Schematic drawing of apparatus used for levitating superheated droplets [123].

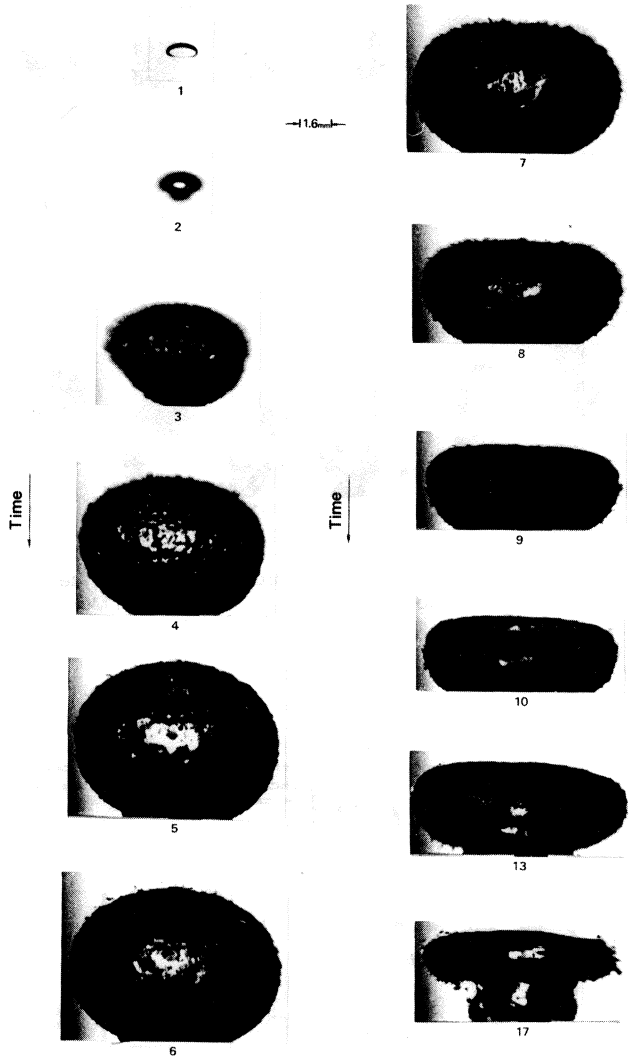

Figure 33. Motion picture sequence of n-butanol droplet boiling in Krytox 143AD (DuPont). $P_0 = 0.101$ MPa, T = 512 K, and framing rate = 2,000 frames/s.

Framing rates corresponding to effective observation times on the order of a millisecond are typical. (Figures 32–34 illustrate the kind of photographic quality of droplets evaporating at their superheat limit one may expect from this method. More will be said about these photographs later.)

Schematic diagrams of two methods used for levitating droplets are shown in Figures 35 and 36 [28, 30, 123, 124]. Droplets were superheated by isothermal decompression (path b-c in Figure 2A) in these apparatuses. The first method (Figure 35) consists of a test section in the shape of a diverging channel placed in a flow loop of liquid 2 driven by an impeller pump. By adjusting the liquid 2

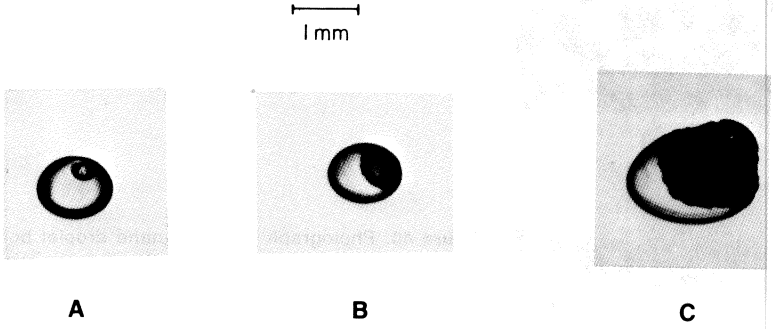

Figure 38. *Photographic sequence of an n-butane droplet boiling in glycerine during the first few microseconds after nucleation at* $P_0 = 0.101$ MPa and $T \simeq 378$ K: (A) $9\mu s < t < 12\ \mu s$, (B) $17\mu s < t < 34\ \mu s$, (C) $55\ \mu s < t < 65\ \mu s$ [18].

the time for complete evaporation progressively increases with pressure. Evaporation of a ~1 mm-diameter droplet takes about four times longer at 1.22 MPa than 0.687 MPa. This fact reflects a strong effect of pressure on bubble growth. The origin of this effect is a combination of reduced influence of dynamic-inertia effects on growth and a decrease in Jakob number, hence temperature difference and heat supply to the bubble, as pressure increases. This reduced growth rate with increasing pressure will also bear on the utility of the spark-gap method of Shepherd and Sturtevant [18] at high pressures. Just how high a pressure the method can be employed before the blast wave intensity created by rapid movement of the bubble boundary diminishes to a value which cannot be detected by the transducer requires further investigation. The precise pressure at which a transition from explosive to nonexplosive vaporization occurs is not known in general, but for n-octane droplets ~1 mm in diameter it appears to be about 4 atm to 6 atm (P_r from 0.24 to 0.33).

The model for bubble growth in droplets developed in the previous section applies under the nonexplosive condition depicted in Figure 32B and C in which the evaporating boundary is also smooth and the bubble does not oscillate. These observations may provide a test of the usefulness of the model presented. Figure 39 shows a comparison between measured [11] and predicted (Section 5) droplet radii ($\bar{S}$) for n-octane. The measurements were sufficiently imprecise to create some

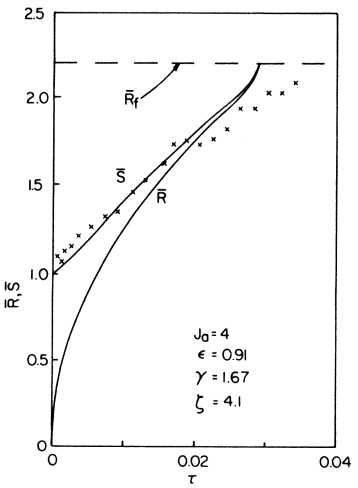

Figure 39. Comparison between calculated [108] and measured [11] droplet radii for an n-octane droplet boiling in glycerine at $P_0 = 1.22$ MPa, $T = 531$ K, and indicated parameters.

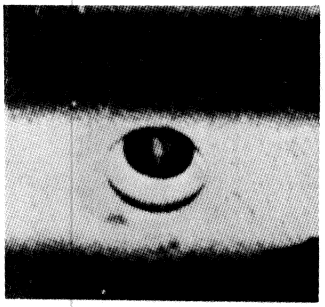

Figure 40. Photograph of an n-butane droplet boiling in water at $P_0 = 0.101$ MPa and a few degrees superheat [128].

uncertainty about the initial droplet size (which enters in the analysis in the definition of τ). Also shown in Figure 39 is the evolution of internal bubble radius ($\bar{R}$), which was not measured. The time domain for the development of a steady vapor temperature and pressure was sufficiently small on the scale of Figure 39 to be undetectable; the data shown correspond to heat-transfer-controlled growth.

Droplets vaporizing at conditions far from their superheat limit occasionally exhibit similarities to high pressure evaporation at the superheat limit. This is shown in Figure 40 which shows evaporation of an n-pentane droplet in water at 0.101 MPa, but only a few degrees superheat [128]. For the droplet nucleation was apparently induced by introducing small gas bubbles or allowing minute amounts of air to dissolve in the droplet. By contrast, the effect of such impurities on an n-octane droplet was minimal (Figures 32b and 32c). It may be noted that the two-phase droplet geometry illustrated in Figure 32 does not correspond to the concentric sphere model which formed the basis of the analysis discussed in the previous section. However, this photograph was taken from the 18th (out of 170) of the sequence illustrated in Figure 32C and corresponded to a time such that only about 10% of the liquid had evaporated. Beyond this time, the liquid sheath becomes increasingly difficult to discern and the assumed geometry provides a better approximation.

CONCLUDING REMARKS

Bubble growth in a liquid droplet at its superheat limit has been reviewed. The problem was divided into two parts:

1. An initial phase during which bubbles form by homogeneous nucleation.
2. A later stage characterized by growth of the initial bubble.

Methods were reviewed for predicting the superheat limits of liquids. This information yields the thermodynamic state of a droplet (its pressure, temperature, and composition) at which the initial bubble is formed in the absence of any extraneous nucleation aids. Subsequent growth of the bubble was analyzed by extending the conventional conservation equations which govern bubble growth in an infinite medium to account for the finite mass of vaporizing liquid. It was shown that the time domain of dynamic effects wherein the bubble gas pressure is still significantly different from the ambient pressure is usually less than a millisecond. Classical analysis will have to be modified to account for bubble oscillations and the wrinkled, nonsmooth, liquid/vapor interface characteristic of explosive boiling.

At present, our understanding of nucleation phenomena outweighs our understanding of the dynamics and heat transfer of bubble growth in droplets. Reliable methods are available for predicting the thermodynamic state of a droplet at which bubbles will form by homogeneous nucleation. A comparatively large data base also exists on the limits of superheat of liquids which forms

the foundation of our confidence in predictive methods. By contrast, a paucity of data exist relating to bubble growth in liquid droplets at the superheat limit. As such, more experiments need to be performed to provide a firmer foundation for more detailed analysis. It is hoped this review stimulates further work on this fundamental and important problem.

Acknowledgments

The author would like to thank Dr. Robert M. Wellek., program director of the Thermodynamics and Transport Phenomenon Program of the National Science Foundation, and Dr. Oscar P. Manley, head of the Engineering Research Program, Office of Basic Energy Sciences of the Department of Energy for their support of this work through grant No. CPE-8106348 and contract No. DE-AC02-83ER13092, respectively.

NOTATION

a	equation of state constant defined by Equation 64
b	equation of state constant
C_1	bubble growth constant (Equation 65a)
c_i	empirical constants defined by Equation 112 (i = 1, 2)
C_{pi}	liquid i (i = 1, 2)
E_n	symbol for a vapor nucleus containing n molecules
F	Helmholtz function
$f_{n,t}$	number density of vapor nuclei containing n molecules at time t
h	heat transfer coefficient
h_{fg}	latent heat of vaporization of liquid 1
$I_{n,t}$	nucleation rate of a nucleus containing n molecules at time t
$k_{f(n)}$	molecular evaporation rate in a nucleus containing n molecules
$k_{r(n)}$	molecular condensation rate in a nucleus containing n molecules
k_i	thermal conductivity of liquid i (i = 1, 2)
k_v	velocity factor (Equation 89)
K	Boltzmann constant
m_i	molecular mass of liquid i (i = 1, 2)
n	number of molecules
n_i	number of molecules of component i in a vapor mixture
n_i^1	number of liquid molecules
n^*	number of molecules in a critical size nucleus
N_n	number density of nuclei in a hypothetical equilibrium state (Equation 50)
N_o	number density of molecules
Nu	Nusselt number
P	pressure of vapor in bubble
P^*	pressure of vapor in a critical size nucleus
P_c	critical pressure
P_{cm}	mixture critical pressure
Pe	Peclet number (Equation 78a)
P_o	ambient (or nucleation) pressure
Pr	Prandtl number
P_r	reduced pressure (= P/P_c)
r	radius
$\bar{r}$	= r/R_o
R	bubble radius
R_f	final bubble radius (Equation 1)
$\mathscr{R}$	gas constant
$\dot{R}$	bubble wall velocity
$\bar{R}$	= R/R_o
$\bar{R}_f$	= R_f/R_o
R_o	initial bubble radius
S	overall droplet radius
S_o	initial overall droplet radius
$\bar{S}$	= S/S_o
$\mathscr{S}$	bubble surface area
t	time
T	temperature
T_c	critical temperature
T_{cm}	mixture critical temperature
T_k	kinetic limit of superheat
T_m	measured kinetic limit of superheat
T_o	ambient (or nucleation) temperature
T_r	reduced temperature (= T/T_c)
T_{roi}	= T_{ki}/T_{ci}
T_t	thermodynamic limit of superheat
T_v	temperature of vapor in bubble
U	internal energy
U_∞	free stream velocity of liquid 1
V	volume
v'	liquid specific volume
x_i	liquid mole fraction of component i in a mixture
y_i	vapor mole fraction of component i
y_i^*	vapor mole fraction of component i in a critical size nucleus

Greek Symbols

α_i	thermal diffusivity of liquid i (i = 1, 2)
γ	$= \alpha_2/\alpha_1$
Γ	defined by Equations 30 and 51
δ	thermal boundary layer thickness
ΔF	change in Helmholtz function
$\Delta\Phi$	minimum energy to form a vapor nucleus
$\Delta\Phi^*$	energy of a critical size nucleus
ε	$= 1 - \rho_v/\rho_1$
$\bar{\varepsilon}$	$= 1 - \rho_1/\rho_2$
ζ	$= k_2/k_1$
η	transformed coordinate variable (Equation 105)
μ'_{ij}	chemical potential of component i in a liquid mixture in system j
μ''_i	chemical potential of component i in a vapor mixture
ρ_i	density of liquid i (i = 1, 2)
ρ_v	vapor density in bubble
σ_i	surface tension of liquid i (i = 1, 2)
σ_{12}	liquid 1/liquid 2 interfacial tension
v	velocity of liquid
Φ	availability (Equation 33)
ω	acentric factor

Subscripts

i	liquid i (i = 1, 2)
s	condition at saturation ($r \to \infty$)

REFERENCES

1. Bankoff, S. G., "Vapor Explosions: A Critical Review." *Proc. 6th Int. Heat Transf. Conf.*, Aug. 7–11 (1978).
2. Henry, R. E., and Fauske, H. K., "Nucleation Processes in Large Scale Vapor Explosion," *J. Heat Transf.*, 101:280 (1979).
3. Reid, R. C., "Rapid Phase Transitions from Liquid to Vapor," in *Advances in Chemical Engineering*, Vol. 12, Academic Press, New York (1983).
4. Lasheras, J. C., Fernandez-Pello, A. C., and Dryer, F. L., "On the Disruptive Burning of Free Droplets of Alcohol/n-Paraffin Solutions and Emulsions" *18th Symp. (Int.) Comb.*, 293 (1981).
5. Dryer, F. L., "Water Addition to Practical Combustion Systems-Concepts and Applications" *16th Symp. (Int.) Comb.*, 279 (1976).
6. Fauske, H. K., "The Role of Nucleation in Vapor Explosions," *Trans. Am. Nuc. Soc.*, 15:813 (1974).
7. Anderson, R. P., and Armstrong, D. P., "R-22 Vapor Explosions," ASME Winter Annual Meeting, Atlanta, Ga, 31 (1977).
8. Buchanan, D. J., and Dullforce, T. A., "Mechanism for Vapour Explosions," *Nature*, 245:32 (1973).
9. Peckover, R. S., Buchanan, D. J., and Ashby, D.E.T.F., "Fuel-Coolant Interactions inSubmarine Vulcanism," *Nature*, 245:307 (1973).
10. Nelson, L. S., and Duda, P. M., "Steam Explosions of Molten Iron Oxide Drops: Easier Initiation at Small Pressurizations," *Nature*, 296:844 (1982).
11. Avedisian, C. T., "Effect of Pressure on Bubble Growth Within Liquid Droplets at the Superheat Limit," *J. Heat Transfer.*, 104:750 (1982).
12. Yang, K., "Explosive Interaction of Liquified Natural Gas and Organic Liquids," *Nature*, 243:221 (1973).
13. Porteous, W. M., and Reid, R. C., "Light Hydrocarbon Vapor Explosions," *Chem. Eng. Prog.*, 72(5):83 (1976).
14. Nakanishi, E., and Reid, R. C., "Liquid Natural Gas-Water Reactions." *Chem. Eng. Prog.*, 67(12):36 (1971).
15. Blander, M., Henstenberg, D., and Katz, J. C., "Bubble Nucleation in n-Pentane, n-Hexane, n-Pentane + n-Hexadecane Mixtures, and Water," *J. Phys. Chem.*, 75:3613 (1971).

16. Jarvis, T. J., Donohue, M. D., and Katz, J. L., "Bubble Nucleation Mechanisms of Liquid Droplets Superheated in Other Liquids," *J. Coll. Inter. Sci.*, 50(2):359 (1975).
17. Avedisian, C. T., and Glassman, I., "Superheating and Boiling of Water in Hydrocarbons at High Pressures," *Int. J. Heat Mass Transf.*, 24(4):695 (1981).
18. Shepherd, J. E., and Sturtevant, B., "Rapid Evaporation at the Superheat Limit," *J. Fluid Mech.*, 121:379 (1982).
19. Buchanan, D. J., "Fuel-Coolant Interaction Theory," *Proc. 4th Int. Heat Transf. Conf.*, 270 (1970).
20. Lasheras, J. C., Yap, L. T., and Dryer, F. L., "The Effect of Ambient Pressure on the Disruptive Vaporization and Burning of Emulsified and Multicomponent Fuel Droplets," Paper No. WSCI 82–94, Western States Section Meeting, Combustion Insitute, Los Angeles, October 11–12, 1982.
21. Sideman, S., and Taitel, Y., "Direct-Contact Heat Transfer with Change of Phase: Evaporation of Drops in an Immiscible Liquid Medium," *Int. J. Heat Mass Transf.*, 7:1273 (1964).
22. Sideman, S., and Isenberg, J., "Direct Contact Heat Transfer with Change of Phase: Bubble Growth in Three-Phase Systems," *Desalination*, 2:207 (1967).
23. Simpson, H. C., Beggs, G. C., and Sohal, M. S., "Nucleation of Butane Drops in Flowing Water," *Proc. 6th Int. Heat Trans. Conf.*, Paper No. PI-10 (1978).
24. Gradon, L., and Selecki, A., "Evaporation of a Liquid Drop Immersed in Another Immiscible Liquid. The case of $\sigma_c < \sigma_d$," *Int. J. Heat Mass Transf.*, 20:459 (1977).
25. Selecki, A., and Gradon, L., "Equation of Motion of an Expanding Vapour Drop in an Immiscible Liquid," *Int. J. Heat Mass Transfer*, 19:925 (1976).
26. Mokhtarzadeh, M. R., and El-Shirbini, A. A., "A Theoretical Analysis of Evaporating Droplets in an Immiscible Liquid," *Int. J. Heat Mass Transf.*, 22:27 (1979).
27. Mori, Y. H., and Komotori, K., "Boiling Modes of Volatile Liquid Drops in an Immiscible Liquid Depending on Degree of Superheat," ASME paper No. 76-HT-13 (1976).
28. Apfel, R. F., and Harbison, J. P., "Acoustically Induced Explosions of Superheat Liquids," *J. Acoust. Soc. Amer.*, 57(6):1371 (1975).
29. Avedisian, C. T., and Glassman, I., "High Pressure Homogeneous Nucleation of Bubbles Within Superheated Binary Liquid Mixtures," *J. Heat Transf.*, 103:272 (1981).
30. Apfel, R. F., "Vapor Cavity Formation in Liquids," Tech. Memo. No. 62, Acoustics Research Laboratory, Harvard University, Cambridge, Mass. (1970).
31. Beams, J. W., "Tensile Strength of Liquid Argon, Helium, Nitrogen, and Oxygen," *Phys. Fluids.*, 2(1):1 (1959).
32. Briggs, L. J., "The Limiting Negative Pressure of Acetic Acid, Benzene, Aniline, Carbon Tetrachloride, and Chloroform," *J. Chem. Phys.*, 19(7):970 (1951).
33. Callen, H. B., *Thermodynamics*, John Wiley, New York, 1960, Chapter 8.
34. Modell, M., and Reid, R. C., *Thermodynamics and Its Applications*, Prentice-Hall, Englewood Cliffs, 1974, Chapter 7.
35. Hildebrand, F. B., *Methods of Applied Mathematics*, Prentice-Hall, Englewood Cliffs, 1965, p. 52.
36. Beegle, B. L., Modell, M., and Reid, R. C., "Thermodynamic Stability Criterion for Pure Substances and Mixtures," *AIChEJ.*, 20(6):1200 (1974).
37. Karimi, A., and Lienhard, J. H., "A Fundamental Equation Representing Water in the Stable Metastable and Unstable States," Electric Power Research Institute Report No. EPRI NP-3328, Project 1438-2, Final Report, December (1983).
38. Temperley, H. N. V., "The Behaviour of Water Under Hydrostatic Tension: III," *Proc. Phys. Soc. Lond.*, 58:199 (1947).
39. Lienhard, J. H., "Correlation for the Limiting Liquid Superheat," *Chem. Eng. Sci.*, 31:847 (1976).
40. Peng, D. Yu, and Robinson, D. B., "A New Two-Constant Equation of State," *Ind. Eng. Chem. Fundam.*, 15(1):59 (1976).
41. Porteous, W., and Blander, M., "Limits of Superheat and Explosive Boiling of Light Hydrocarbons, Halocarbons, and Hydrocarbon Mixtures," *AIChEJ* 21(3):560 (1975).
42. Frenkel, J., *Kinetic Theory of Liquids*, Oxford U. P., Oxford, 1946, pp. 382–400.

43. Gibbs, J. W., *Collected Works*, Vol. 1, Longmans, Green, New York, 1928.
44. Skripov, V. R., and Sinitsyn, E. N., "Nucleation in Superheated Liquids and Surface Tension," 42:167 (1968).
45. Katz, J. L., "Condensation of A Supersaturated Vapor. I. The Homogeneous Nucleation of the n-Alkanes," *J. Chem. Phys.*, 52(9):4733 (1970).
46. Keenan, J. H., *Thermodynamics*, John Wiley, New York, 1941, Chapter 17.
47. Pinnes, E. C., and Mueller, W. K., "Homogeneous Vapor Nucleation and Superheat Limits of Liquid Mixtures," *J. Heat Transf.*, 101:617 (1979).
48. Holden, B. C., and Katz, J. C., "The Homogeneous Nucleation of Bubbles in Superheated Binary Liquid Mixtures," *AIChEJ*, 24(2):260 (1978).
49. Volmer, M., *Kinetics of Phase Formation*, translated by Intelligence Department, ATI No. 81935 (F-TS-7068-RE) from the clearinghouse for Federal and Technical Information.
50. Reiss, H., "The Kinetics of Phase Transitions in Binary Systems," *J. Chem. Phys.*, 18(6):840 (1950).
51. Turnbull, D., and Fisher, J. C., "Rate of Nucleation in Condensed Systems," *J. Chem. Phys.*, 17(1):71 (1949).
52. Farley, F. J. M., "The Theory of the Condensation of Supersaturated Ion-Free Vapour," *Proc. Roy. Soc. Lond.*, A212:530 (1952).
53. McDonald, J. E., "Homogeneous Nucleation of Vapor Condensation. II, Kinetic Aspects," *Am. J. Phys.*, 31:31 (1963).
54. Katz, J. L., Saltsburg, H., and Reiss, H., "Nucleation in Associated Vapors," *J. Coll. Inter. Sci.*, 21:560 (1966).
55. Hirschelder, J. O., "Kinetics of Homogeneous Nucleation on Many-Component Systems," *J. Chem. Phys.*, 61(7):2690 (1974).
56. Stauffer, D., "Kinetic Theory of Two-Component ("Hetero-Molecular") Nucleation and Condensation," *J. Aerosol. Sci.*, 7:319 (1976).
57. Katz, J. L., and Wiedersich, H., "Nucleation Theory without Maxwell Demons," *J. Coll. Inter. Sci.*, 61(2):351 (1977).
58. Katz, J. L., and Donohue, M. D., "A Kinetic Approach to Homogeneous Nucleation Theory," in *Advances in Chemical Physics*, 40:137 (1979).
59. Springer, G. S., "Homogeneous Nucleation," in *Advances in Heat Transfer*, 14:281 (1978).
60. Vega, E., and Peters, L. K., "Dynamics of Cluster Growth During Homogeneous Nucleation of Supersaturated Vapors," *Aerosol. Sci. Tech.*, 2:513 (1983).
61. Andres, R. P., and Boudart, M., "Time Lag in Multistate Kinetics: Nucleation," *J. Chem. Phys.*, 42(6):2057 (1965).
62. Cohen, E. R., "The Accuracy of the Approximations in Classical Nucleation Theory," *J. Stat. Phys.*, 2(2):147 (1970).
63. Katz, J. L., "The Critical Supersaturations Predicted by Nucleation Theory," *J. Stat. Phys.*, 2(2):137 (1970).
64. Avedisian, C. T., "The Homogeneous Nucleation Limits of Liquids," *J. Phys. Chem. Ref. Data.*, 14(3):695 (1985).
65. Skripov, V. P., and Erinakov, F. C., "Pressure Dependence of the Limiting Superheating of a Liquid," *Russ. J. Phys. Chem.*, 38(2):208 (1964).
66. Lienhard, J. H., and Karimi, A., "Homogeneous Nucleation and the Spinodal Line," *J. Heat Transf.*, 103:61 (1981).
67. Pavlov, P. A., and Skripov, V. P., "Kinetics of Spontaneous Nucleation in Strongly Heated Liquids," *High Temp.*, 8:540 (1970).
68. Skripov, V. P., *Superheated Liquids*, John Wiley, New York, 1974.
69. Lienhard, J. H., and Karimi, A., "Corresponding States Correlations of the Liquid and Vapor Spinodal Lines," ASME Paper No. 77-HT-20. (1977).
70. Prausnitz, J. M., *Molecular Thermodynamics of Fluid-Phase Equilibration*, Prentice-Hall, Englewood Cliffs, 1969, pp. 69–73.
71. Guggenhiem, E. A., "The Principle of Corresponding States," *J. Chem. Phys.*, 13(7):253 (1945).

72. Lienhard, J. H., "Corresponding States Correlations of the Spinodal and Homogeneous Nucleation Limits," *J. Heat Transf.*, 104:379 (1982).
73. Apfel, R. E., "Vapor Nucleation at a Liquid-Liquid Interface," *J. Chem. Phys.*, 54(1):62 (1971).
74. Avedisian, C. T., and Sullivan, J. R., "A Generalized Corresponding States Method for Predicting the Limits of Superheat of Mixtures: Application to the Normal Alcohols," *Chem. Eng. Sci.*, 39(6):1033–1042 (1984).
75. Bankoff, S. G., "Diffusion Controlled Bubble Growth," in *Advances in Chemical Engineering*, Vol. 6, Academic Press, New York (1966).
76. Prosperetti, A., and Plesset, M., "Vapour-Bubble Growth in a Superheated Liquid," *J. Fluid Mech.*, 85(2):349 (1978).
77. Scriven, L. E., "On the Dynamics of Phase Growth," *Chem. Eng. Sci.*, 10:1 (1959).
78. Chambré, P. L., "On the Dynamics of Phase Growth," *Quart. J. Mech. Appl. Math.*, 9(2):224 (1956).
79. Rayleigh, Lord, "On the Pressure Developed in a Liquid During the Collapse of a Spherical Cavity," *Philos. Mag.*, 34:94 (1917).
80. Bornhorst, W. J., and Hatsopoulos, G. N., "Bubble Growth Calculation Without Neglect of Interfacial Discontinuities," *J. Appl. Mech.*, 34:847 (1967).
81. Theofanous, T. G., et al., "A Theoretical Study on Bubble Growth in Constant and Time Dependent Pressure Fields," *Chem. Eng. Sci.*, 24:885 (1969).
82. Mikic, B. B., Rohsenow, W. M., and Griffith, P., "On Bubble Growth Rates," *Int. J. Heat Mass Transf.*, 13:657 (1970).
83. Plesset, M. S., and Zwick, S. A., "The Growth of Vapor Bubbles in Superheated Liquids," *J. Appl. Phys.*, 25(4):493 (1954).
84. Plesset, M., and Prosperetti, A., "Bubble Dynamics and Cavitation," *Ann. Rev. Fluid. Mech.*, 9:145 (1977).
85. Forster, H. K., and Zuber, N., "Growth of a Vapor Bubble in a Superheated Liquid," *J. Appl. Phys.*, 25(4):474 (1954).
86. Birkhoff, G., Margulies, R. S., and Horning, W. A., "Spherical Bubble Growth," *Phys. Fluids*, 1:201 (1958).
87. Moalem-Maron, D., and Zijl, W., "Growth, Condensation, and Departure of Small and Large Vapour Bubbles in Pure and Binary Systems," *Chem. Eng. Sci.*, 33:1339 (1978).
88. Saitoh, T., and Shima, A., "Numerical Solution for the Spherical Bubble Growth Problem in a Uniformly Ultraheated Liquid," *J. Mech. Eng. Sci.*, 19(3):101 (1977).
89. Aguila, F., and Thompson, S., "Nonequilibrium Flashing Model for Rapid Pressure Transients," ASME Paper No. 81-HT-35 (1981).
90. Dalle-Donne, M., and Ferranti, M. P., "The Growth of Vapor Bubbles in Superheated Sodium," *Int. J. Heat Mass Transf.*, 18:901 (1975).
91. Bankoff, S. G., and Choi, H. K., "Growth of a Bubble at a Heated Surface in a Pool of Liquid Metal," *Int. J. Heat Mass Transf.*, 19:87 (1976).
92. Cha, Y. S., and Henry, R. E., "Bubble Growth During Decompression of a Liquid," *J. Heat Transf.*, 103:56 (1981).
93. Theofanous, T. G., and Patel, P. D., "Universal Relations for Bubble Growth," *Int. J. Heat Mass Transf.*, 19:425 (1976).
94. Van Stralen, S. J. D., and Cole, R., *Boiling Nucleation*, Vol. 1, Hemisphere, New York, 1979, Chapter 3.
95. Moore, G. R., "Vaporization of Superheated Drops in Liquids," *AIChEJ.*, 5(4):458 (1959).
96. Blander, M., and Katz, J. L., "Bubble Nucleation in Liquids," *AIChEJ.* 21(5):833 (1975).
97. Avedisian, C. T., and Andres, R. P., "Bubble Nucleation in Superheated Liquid-Liquid Emulsions," *J. Coll. Interf. Sci.*, 64(3):438 (1978).
98. Burdon, R. S., *Surface Tension and the Spreading of Liquids*, Cambridge U. P., Cambridge, 1949.
99. Jongenelen, F. C. H., Groeneweg, F., and Gouda, J. H., "Effects of Interfacial Forces on the Evaporation of a Superheated Water Droplet in a Hot Immiscible Oil," *Chem. Eng. Sci.*, 33:777 (1978).

100. Tochitani, Y., et al., "Vaporization of Single Liquid Drops in an Immiscible Liquid Part II: Heat Transfer Characteristics," *Wärme-und Stoffübertragung*, 10:71 (1977).
101. Moalem-Maron, D., Skolov, M., and Sideman, S., "A Closed Periodic Condensation-Evaporation Cycle of an Immiscible, Gravity Driven Bubble," *Int. J. Heat Mass Transf.*, 23:1417 (1980).
102. Tokuda, N., Yang, W. J., and Clark, J. A., "Dynamics of Moving Gas Bubbles in Injection Cooling," *J. Heat Transf.*, 90:371 (1968).
103. Ruckenstein, E., and Davis, E. J., "The Effects of Bubble Translation on Vapor Bubble Growth in a Superheated Liquid," *Int. J. Heat Mass Transf.*, 14:939 (1971).
104. Sidman, D., "Direct Contact Heat Transfer Between Immiscible Liquid Drops," in *Advances in Chemical Engineering*, Vol. 6, Academic Press, New York.
105. Isenberg, J., and Sideman, S., "Direct Contact Heat Transfer with Change of Phase" Bubble Condensation in Immiscible Liquid," *Int. J. Heat Mass Transf.*, 13:997 (1970).
106. Duda, J. L., Malone, M. F., and Notter, R. H., "Analysis of Two-Dimensional Diffusion-Controlled Moving Boundary Problems," *Int. J. Heat Mass Transf.*, 18:901 (1975).
107. Saitoh, T., "Numerical Method for Multidimensional Freezing Problems in Arbitrary Domains," *J. Heat Mass Transf.*, 100:294 (1978).
108. Suresh, K., "Vaporization of a Superheated Liquid Drop," M.S. thesis, Cornell University (1984).
109. Jacobs, H. R., and Cook, D. S., "Direct Contact Condensation on a Non-Circulating Drop," *Proc. 6th Int. Heat Transf. Conf.*, paper No. CS-2 (1978).
110. Strenge, P. H., Orell, A., and Westwater, J. W., "Microscopic Study of Bubble Growth During Nucleation Boiling," *AIChEJ.*, 7(4):579 (1961).
111. Landau, L. D., "On the Theory of Slow Combustion," *Acta Physioch.*, 19:77 (1974).
112. Apfel, R. E., "Water Superheated to 279.5°C at Atmospheric Pressure," *Nature Phys. Sci.*, 238:63 (1972).
113. Apfel, R. E., "Tensile Strength of Superheated n-Hexane Droplets," *Nature Phys. Sci.*, 233:119 (1971).
114. Ermakov, G. V., and Skripov, V. P., "Experimental Test of the Theory of Homogeneous Nucleus Formation in Superheated Liquids," *Russ. J. Phys. Chem.*, 43(9):1242 (1969).
115. Ermakov, G. V., and Skripov, V. P., "Saturation Five, Critical Parameters, and the Maximum Degree of Superheating of Perfluoro-Paraffins, " *Russ. J. Phys. Chem.*, 41(1):39 (1967).
116. Eberhart, J. G., Kremsner, W., and Blander, M., "Metastability Limits of Superheated Liquids: Bubble Nucleation Temperatures of Hydrocarbons and their Mixtures," *J. Coll. Interf. Sci.*, 50(2):369 (1975).
117. Renner, T. A., Kucera, G. H., and Blander, M., "Explosive Boiling in Light Hydrocarbons and their Mixtures," *J. Col. Interf. Sci.*, 52(2):391 (1975).
118. Patrick, J. R., and Reid, R. C., "Superheat-Limit Temperatures of Polar Liquids," *Ind. Eng. Chem. Fundam.*, 20(4):315 (1981).
119. Skripov, V. P., and Ermakov, G. V., "The Limit of Superheating of Liquids," 37(8):1047 (1963).
120. Patrick-Yeboah, J. R., "Superheat Limit Temperatures for Nonideal Liquid Mixtures and Pure Components," Ph.D. Thesis, Massachusetts Institute of Technology (1979).
121. Wakeshima, H., and Takata, K., "On the Limit of Superheat," *J. Phys. Soc. Japan*, 13(11):1398 (1958).
122. Skripov, V. P., and Kukushkin, V. I., "Apparatus for Observing the Superheating Limits of Liquids," *Russ. J. Phys. Chem.*, 35(12):1393 (1961).
123. Forest, T. W., and Ward, C. A., "Effect of a Dissolved Gas on the Homogeneous Nucleation Pressure of a Liquid," *J. Chem. Phys.*, 66(6):2322 (1977).
124. Forest, T. W., and Ward, C. A., "Homogeneous Nucleation of Bubbles in Solutions at Pressures above the Vapor Pressure of the Pure Liquid," *J. Chem. Phys.*, 69(5):2221 (1978).
125. Mori, Y. H., and Komotori, K., "Boiling of Single Superheated Drops in an Immiscible Liquid," *Heat Transf-Japanese Res.*, 5(3):75 (1976).
126. Dufour, L., "Sur L'Ebullition des Liquides," *Comptes Rendus*, 52:986, Jan.-June (1861).
127. Dufour, L., "Sur L'Ebullition des Liquides," *Comptes Rendus*, 53:846, July-Dec. (1861).
128. Sideman, S., "Photography of Drops in Liquid Media," 19(6):426 (1966).